Publication Year	2011
Acceptance in OA	2023-01-18T10:17:43Z
Title	The long-lasting activity of 3C 454.3: GASP-WEBT and satellite observations in 2008-2010
Authors	RAITERI, Claudia Maria, VILLATA, Massimo, Aller, M.F., Gurwell, M.A., Kurtanidze, O.M., Lähteenmäki, A., Larionov, V.M., Romano, P., VERCELLONE, STEFANO, Agudo, I., Aller, H.D., Arkharov, A.A., Bach, U., Benítez, E., Berdyugin, A., Blinov, D.A., Borisova, E.V., Böttcher, M., Bravo Calle, O.J.A., BUEMI, CARLA SIMONA, Calcidese, P., Carosati, D., Casas, R., Chen, W.-P., Efimova, N.V., Gómez, J.L., Gusbar, C., Hawkins, K., Heidt, J., Hiriart, D., Hsiao, H.Y., Jordan, B., Jorstad, S.G., Joshi, M., Kimeridze, G.N., Koptelova, E., Konstantinova, T.S., Kopatskaya, E.N., Kurtanidze, S.O., Larionova, E.G., Larionova, L.V., LETO, PAOLO, Li, Y., Ligustri, R., Lindfors, E., Lister, M., Marscher, A.P., Molina, S.N., Morozova, D.A., Nieppola, E., Nikolashvili, M.G., Nilsson, K., Palma, N., Pasanen, M., Reinthal, R., Roberts, V., Ros, J.A., Roustazadeh, P., Sadun, A.C., Sakamoto, T., Schwartz, R.D., Sigua, L.A., Sillanpää, A., Takalo, L.O., Tammi, J., Taylor, B., Tornikoski, M., TRIGILIO, CORRADO, Troitsky, I.S., UMANA, Grazia Maria Gloria, Volvach, A., Yuldasheva, T.A.
Publisher's version (DOI)	10.1051/0004-6361/201117026
Handle	http://hdl.handle.net/20.500.12386/32908
Journal	ASTRONOMY & ASTROPHYSICS
Volume	534

A&A 534, A87 (2011)
DOI: 10.1051/0004-6361/201117026

Astronomy & Astrophysics

The long-lasting activity of 3C 454.3

GASP-WEBT and satellite observations in 2008–2010⋆,⋆⋆

C. M. Raiteri[1], M. Villata[1], M. F. Aller[2], M. A. Gurwell[3], O. M. Kurtanidze[4], A. Lähteenmäki[5], V. M. Larionov[6,7,8], P. Romano[9], S. Vercellone[9], I. Agudo[10,11], H. D. Aller[2], A. A. Arkharov[7], U. Bach[12], E. Benítez[13], A. Berdyugin[14], D. A. Blinov[6,8], E. V. Borisova[6], M. Böttcher[15], O. J. A. Bravo Calle[6], C. S. Buemi[16], P. Calcidese[17], D. Carosati[18,19], R. Casas[20,21], W.-P. Chen[22], N. V. Efimova[6,7], J. L. Gómez[10], C. Gusbar[15], K. Hawkins[15], J. Heidt[23], D. Hiriart[13], H. Y. Hsiao[24,22], B. Jordan[25], S. G. Jorstad[11,6], M. Joshi[11], G. N. Kimeridze[4], E. Koptelova[22,26], T. S. Konstantinova[6], E. N. Kopatskaya[6], S. O. Kurtanidze[4], E. G. Larionova[6], L. V. Larionova[6], P. Leto[16], Y. Li[15], R. Ligustri[27], E. Lindfors[14], M. Lister[28], A. P. Marscher[11], S. N. Molina[10], D. A. Morozova[6], E. Nieppola[5,29], M. G. Nikolashvili[4], K. Nilsson[29], N. Palma[15,30], M. Pasanen[14], R. Reinthal[14], V. Roberts[15], J. A. Ros[21], P. Roustazadeh[15], A. C. Sadun[31], T. Sakamoto[32], R. D. Schwartz[33], L. A. Sigua[4], A. Sillanpää[14], L. O. Takalo[14], J. Tammi[5], B. Taylor[11,34], M. Tornikoski[5], C. Trigilio[16], I. S. Troitsky[6], G. Umana[16], A. Volvach[35], and T. A. Yuldasheva[6]

(Affiliations can be found after the references)

Received 5 April 2011 / Accepted 24 June 2011

ABSTRACT

Context. The blazar 3C 454.3 is one of the most active sources from the radio to the γ-ray frequencies observed in the past few years.

Aims. We present multiwavelength observations of this source from April 2008 to March 2010. The radio to optical data are mostly from the GASP-WEBT, UV and X-ray data from Swift, and γ-ray data from the AGILE and *Fermi* satellites. The aim is to understand the connection among emissions at different frequencies and to derive information on the emitting jet.

Methods. Light curves in 18 bands were carefully assembled to study flux variability correlations. We improved the calibration of optical-UV data from the UVOT and OM instruments and estimated the Lyα flux to disentangle the contributions from different components in this spectral region.

Results. The observations reveal prominent variability above 8 GHz. In the optical-UV band, the variability amplitude decreases with increasing frequency due to a steadier radiation from both a broad line region and an accretion disc. The optical flux reaches nearly the same levels in the 2008–2009 and 2009–2010 observing seasons; the mm one shows similar behaviour, whereas the γ and X-ray flux levels rise in the second period. Two prominent γ-ray flares in mid 2008 and late 2009 show a double-peaked structure, with a variable γ/optical flux ratio. The X-ray flux variations seem to follow the γ-ray and optical ones by about 0.5 and 1 d, respectively.

Conclusions. We interpret the multifrequency behaviour in terms of an inhomogeneous curved jet, where synchrotron radiation of increasing wavelength is produced in progressively outer and wider jet regions, which can change their orientation in time. In particular, we assume that the long-term variability is due to this geometrical effect. By combining the optical and mm light curves to fit the γ and X-ray ones, we find that the γ (X-ray) emission may be explained by inverse-Comptonisation of synchrotron optical (IR) photons by their parent relativistic electrons (SSC process). A slight, variable misalignment between the synchrotron and Comptonisation zones would explain the increased γ and X-ray flux levels in 2009–2010, as well as the change in the γ/optical flux ratio during the outbursts peaks. The time delays of the X-ray flux changes after the γ, and optical ones are consistent with the proposed scenario.

Key words. galaxies: active – quasars: general – quasars: individual: 3C 454.3 – galaxies: jets

1. Introduction

A relativistic jet pointing at a small angle to the line of sight is most likely responsible for the extreme properties of the active galactic nuclei known as “blazars”, i.e. BL Lac objects and flat-spectrum radio quasars (FSRQ). Indeed, the alignment would cause Doppler enhancement of the emission and contraction of its variability time scales. This peculiar orientation would also explain the apparent superluminal motion of radio knots in the jet. Owing to the jet emission beaming, we observe intensified synchrotron radiation from the radio to the UV–X-ray band and inverse-Compton radiation at higher energies, up to the TeV domain. Sometimes, in low brightness states, other contributions are detected, likely because of unbeamed radiation from the blazar nucleus, i.e. the accretion disc and broad line region (BLR). This occurs more often in FSRQ than in BL Lac objects, and indeed the classical distinction between the two classes is based on the equivalent width of their broad emission lines (that has to be greater than 5 Å in the rest frame for FSRQ). One of the main issues concerns the origin of the seed photons that are Comptonised to X- and γ-ray energies: relativistic electrons certainly upscatter the soft photons they have previously produced by synchrotron emission (synchrotron-self-Compton, or SSC, process), but possibly also photons coming from outside the jet (external Compton, or EC, process), in particular from the accretion disc, the BLR, or an obscuring torus (see e.g. Dermer et al. 2009, and references therein).

The quasar-type blazar 3C 454.3 has received particular attention by the international astronomical community since it underwent a major outburst in 2005 (Villata et al. 2006; Giommi et al. 2006; Pian et al. 2006; Fuhrmann et al. 2006). Indeed,

---

⋆ The radio-to-optical data presented in this paper are stored in the GASP-WEBT archive; for questions regarding their availability, please contact the WEBT President Massimo Villata (`villata@oato.inaf.it`).

⋆⋆ Table 3 is available in electronic form at `http://www.aanda.org` after many decades of intense radio, but only mild optical activity, the source began brightening in the optical band in 2001, until in May 2005 it reached the maximum optical level ever observed, $R = 12.0$. The outburst was simultaneously detected also in X-rays, while the millimetric radio flux peaked about one month after, and the 15–43 GHz flux much later (Villata et al. 2007; Raiteri et al. 2008b). According to Villata et al. (2006, 2007) the observed change in behaviour starting from 2001 was a geometric effect, i.e. the motion of a curved jet producing variations in the viewing angle of the different emitting regions.

In the following 2006–2007 observing season the source remained in a faint state, and new features appeared in its spectral energy distribution (SED). Through the analysis of low-energy data from the Whole Earth Blazar Telescope[1] (WEBT) and high-energy data from the *XMM-Newton* satellite, Raiteri et al. (2007) were able to recognise both a little blue bump in the optical, possibly due to emission lines from the BLR, and a UV excess, suggesting a big blue bump likely due to thermal radiation from the accretion disc. Moreover, they argue that the X-ray spectrum may be concave, with spectral softening at lower energies becoming more evident when the source is fainter, maybe revealing the high-frequency tail of the big blue bump. Finally, they ascribed the flux excess in the J band to a prominent broad Hα emission line. Both the UV excess and X-ray spectral curvature were also inferred from further *XMM-Newton* observations, at the beginning of the following observing season, while the contribution of the Hα line was confirmed by near-IR spectroscopy at Campo Imperatore (Raiteri et al. 2008b).

Then, from July 2007 the source began a new activity phase, during which it was detected several times in γ-rays by the AGILE satellite[2], and was monitored from the optical to the radio bands by the WEBT and its GLAST-AGILE Support Program (GASP, Villata et al. 2008). The results of these observations were published in Vercellone et al. (2008), Raiteri et al. (2008a,b), Vercellone et al. (2009), Donnarumma et al. (2009), Villata et al. (2009a), and Vercellone et al. (2010). Rotations of the optical polarisation vector both clockwise and counterclockwise were detected by Sasada et al. (2010). In contrast, observations at very high energies ($E > 100$ GeV) by the Cherenkov telescope MAGIC resulted in only upper limits (Anderhub et al. 2009).

From the theoretical point of view, Ghisellini et al. (2007) compare the source SED of July 2007 with that of May 2005 and infer that the dissipation site in relativistic jets changes, with more compact emitting regions, smaller bulk Lorentz factors, and greater magnetic fields characterising locations closer to the black hole. However, in the Ghisellini et al. (2007) view, the dissipation always occurs in a subparsec zone, where the seed photons for Compton emission are provided by the BLR. In contrast, Sikora et al. (2008) claim that the dissipation region is located much farther, in the millimetric photosphere, at some parsecs from the central engine, so the Compton emission is due to scattering of infrared photons emitted by the hot dust.

In the meanwhile, the *Fermi* satellite[3] was launched, providing an unprecedented monitoring of 3C 454.3 at γ-ray energies (Bonning et al. 2009; Abdo et al. 2009). The data from AGILE and *Fermi* were separately used to study the correlations between flux variations in optical and γ-rays. All results agreed that the time lag of γ-ray flux variations after the optical ones is less than one day (Vercellone et al. 2009; Donnarumma et al. 2009; Bonning et al. 2009; Vercellone et al. 2010). Finke & Dermer (2010) discuss the spectral break at ~2.4 GeV shown by *Fermi* data in August 2008 suggesting that it results from the combination of Compton-scattered disc and BLR radiations.

An analysis of the radio-optical data in 2005–2007, including space observations by *Spitzer* in the infrared, revealed two synchrotron peaks, the primary at IR and the secondary at sub-mm wavelengths, likely arising from distinct regions in the jet (Ogle et al. 2011).

A multiwavelength study of the flaring behaviour of 3C 454.3 during 2005–2008 was performed by Jorstad et al. (2010). These authors suggest that the emergence of a superluminal knot from the core produces a series of optical and high-energy outbursts, and that the millimetre-wave core lies at the end of the jet acceleration and collimation zone.

Suzaku observations of 3C 454.3 in November 2008 analysed by Abdo et al. (2010) confirmed the earlier suggestions by Raiteri et al. (2007, 2008b) that there seems to be a soft X-ray excess, which becomes more important when the source gets fainter. They interpret it as either a contribution of the high-energy tail of the synchrotron component or bulk-Compton radiation produced by Comptonisation of UV photons from the accretion disc by cold electrons in the innermost parts of the relativistic jet.

More recently, Pacciani et al. (2010; see also Striani et al. 2010) have reported on a γ-ray flare of 3C 454.3 detected by AGILE in December 2009, when the peak flux reached 2.0×10^{-5} photons cm^{-2} s^{-1}. The simultaneous flux increase at UV and optical frequencies was by far less dramatic. The authors found that the source behaviour during the flare cannot be accounted for by a simple one-zone model, but an additional particle component is needed. In contrast, Bonnoli et al. (2011) explain the source behaviour in the same period by means of a one-zone model, where the magnetic field is slightly weaker when the overall jet luminosity is higher. A new intense γ-ray flare was detected by *Fermi* in April 2010 ($\approx 1.6 \times 10^{-5}$ photons cm^{-2} s^{-1}, Ackermann et al. 2010), when fast variability on a time scale of a few hours was revealed (Foschini et al. 2010), supporting earlier results by Tavecchio et al. (2010), who claim that the dissipation region must be close to the black hole. The December 2009 and April 2010 γ-ray outbursts detected by *Fermi* were further analysed by Ackermann et al. (2010). These authors in particular discuss the observed spectral break at a few GeV, which they ascribe to a break in the underlying electron spectrum. This feature was also observed during the unprecedented γ-ray outburst of November 2010 (Abdo et al. 2011), when the γ flux rose to $(6.6 \pm 0.2) \times 10^{-5}$ photons cm^{-2} s^{-1} showing clear spectral changes.

In this paper we present the radio-to-optical monitoring results obtained by the GASP-WEBT in 2008–2010, together with UV and X-ray data acquired by Swift and γ-ray observations by the AGILE and *Fermi* satellites. We analyse the flux correlations at different frequencies to derive information on the jet physics and structure. As in several previous WEBT-GASP papers, we focus on an interpretation of the observed light curves in terms of variations in the orientation and curvature of an inhomogeneous emitting jet.

2. GASP-WEBT observations

The GLAST-AGILE Support Program (GASP) was born in 2007 as a project of the WEBT. Its aim is to perform long-term multifrequency monitoring of selected γ-loud blazars during the

---

[1] `http://www.oato.inaf.it/blazars/webt/`

[2] `http://agile.iasf-roma.inaf.it/`

[3] `http://fermi.gsfc.nasa.gov/`

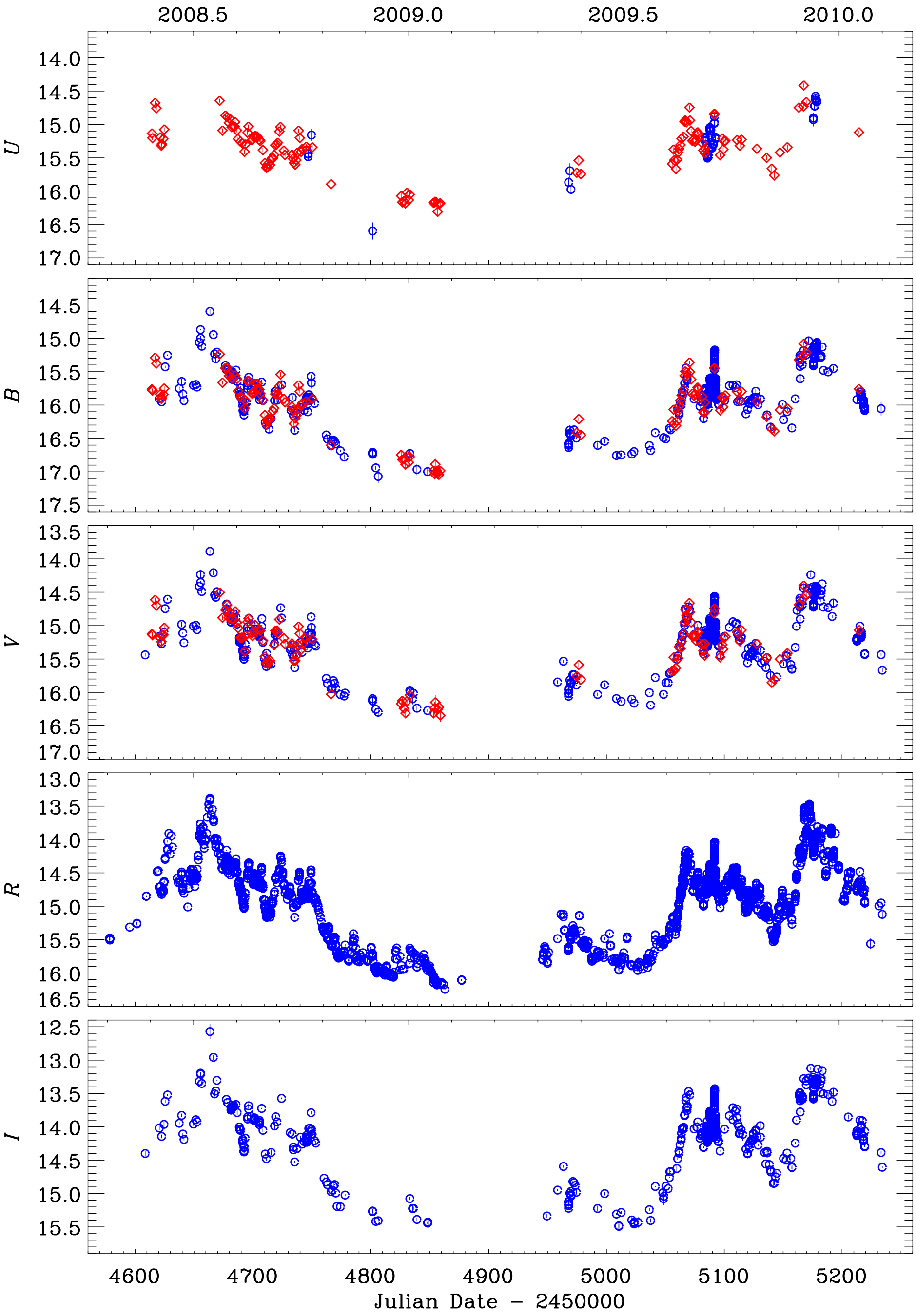

Fig. 1. Optical light curves of 3C 454.3 in 2008–2010 built with GASP-WEBT data (blue circles) and Swift-UVOT data (red diamonds). The UVOT points have been shifted to match the ground-based data (see text for details).

operation of the AGILE and *Fermi* (formerly GLAST) γ-ray satellites. In the optical, data are collected in the R band, and photometric calibration of 3C 454.3 is obtained with respect to Stars 1, 2, 3, and 4 by Raiteri et al. (1998). For this paper we also collected data taken by the GASP-WEBT observers in other optical bands to obtain spectral information.

Figure 1 shows the optical light curves of 3C 454.3 in 2008–2010. The 2008–2009 R-band light curve has already been published by Villata et al. (2009a). GASP-WEBT observations in 2009–2010 were performed at the following observatories: Abastumani, Calar Alto[4], Crimean, Galaxy View, Goddard (GRT), Kitt Peak (MDM), Lowell (Perkins), Lulin, New Mexico Skies, Roque de los Muchachos (KVA), Sabadell, San Pedro Martir, St. Petersburg, Talmassons, Teide (BRT), Tijarafe, and Valle d'Aosta. The figure also displays optical data acquired by the UVOT instrument onboard the Swift satellite (see Sect. 3).

Both observing seasons are characterised by intense activity, with several flaring episodes superimposed on prominent outbursts. The total variation amplitude is similar in the two seasons and it increases with increasing wavelength, as already noticed in previous works (e.g. Villata et al. 2006; Raiteri et al. 2008b). This feature was interpreted as an effect of an additional, stabler, emission component, mainly contributing to the blue part of the optical spectrum. This radiation likely comes from the accretion disc and BLR (see also Sects. 3 and 4). Noticeable

---

[4] Calar Alto data were acquired as part of the MAPCAT project: `http://www.iaa.es/~iagudo/research/MAPCAT`

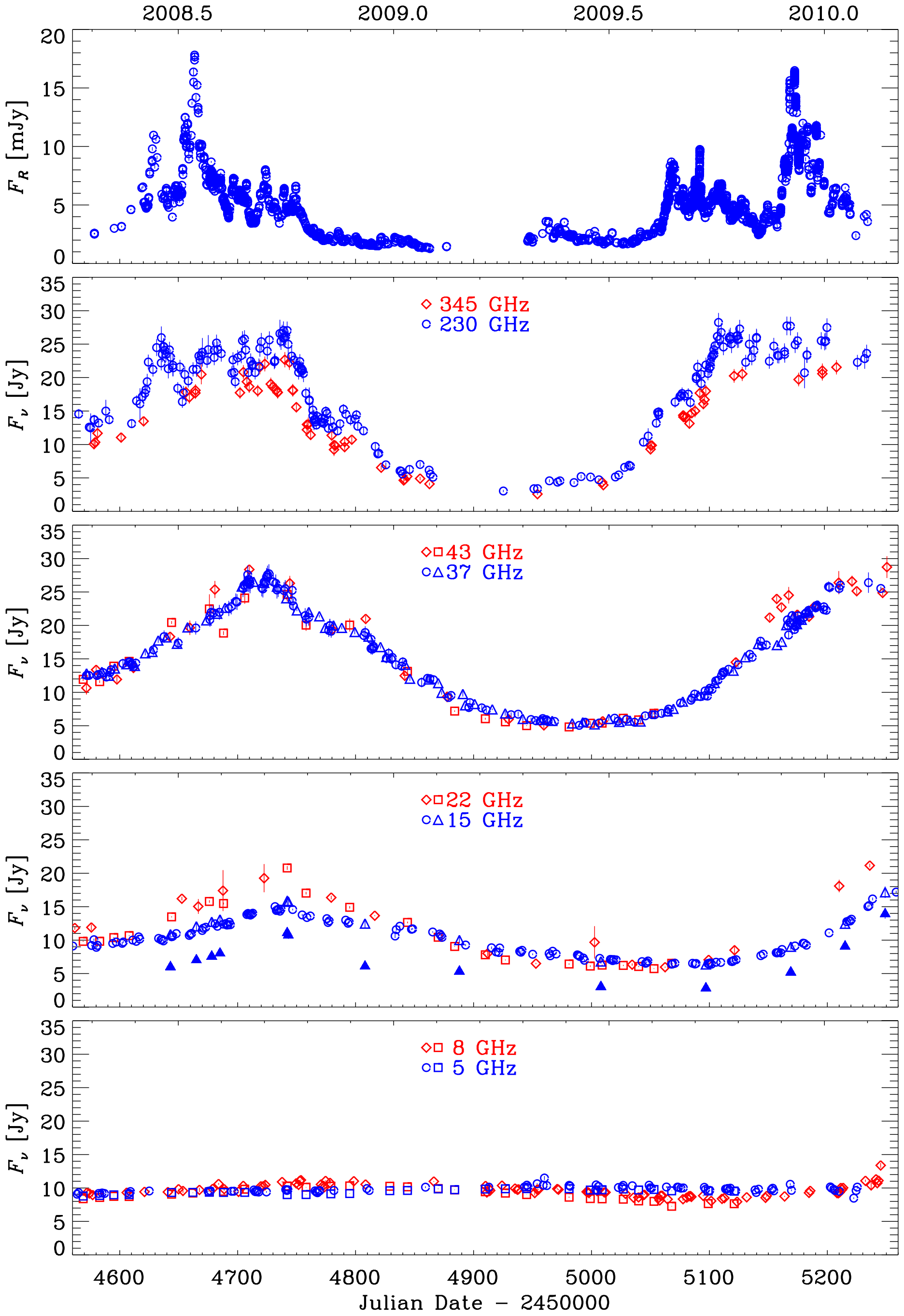

Fig. 2. *R*-band optical flux densities in 2008–2010 (*top*) compared to the radio light curves at different frequencies. The GASP data (blue circles and red diamonds) are complemented with those from the Crimean Observatory at 37 GHz (blue triangles) and with those from the VLA/VLBA Polarization Calibration Database at 43, 22, 8 GHz (red squares), and at 5 GHz (blue squares). Data at 15 GHz from the MOJAVE Program are also included as blue triangles: the filled ones represent the core flux, and the empty ones the total flux.

fast variability episodes are observed; in particular, a 0.3 mag brightening in about six hours on JD = 2 455 066 and 2 455 091, and a 0.5 mag brightening in about 14 h, from JD = 2 455 171.6 to 2 455 172.2.

The radio light curves of 3C 454.3 at different wavelengths in 2008–2010 are displayed in Fig. 2. Observations at 230 and 345 GHz are from the Submillimeter Array (SMA[5]), a radio interferometer including eight dishes of 6 m size located atop Mauna Kea, in Hawaii. Data at longer wavelengths were taken at the radio telescopes of Medicina (5, 8, and 22 GHz), Metsähovi (37 GHz), Noto (43 GHz), and UMRAO (4.8, 8.0, and 14.5 GHz). The Crimean Observatory provided additional observations at 37 GHz. We also included data from the VLA/VLBA Polarization Calibration Database[6] and from the MOJAVE programme[7].

---

[5] These data were obtained as part of the normal monitoring programme initiated by the SMA (see Gurwell et al. 2007).

[6] `http://www.vla.nrao.edu/astro/calib/polar/`. Data in the period between JD = 2 455 110 and 2 455 190 at 43 and 22 GHz, and between JD = 2 455 130 and 2 455 190 at 8 and 5 GHz were affected by problems in the automatic reduction procedure (Steven Myers, priv. comm.) and were thus removed.

[7] `http://www.physics.purdue.edu/astro/MOJAVE/`

In the top panel of Fig. 2 the R-band flux densities are shown for comparison. They were obtained by correcting magnitudes for a Galactic extinction of 0.29 mag and then converting them into fluxes using the absolute fluxes by Bessell et al. (1998).

At 230 GHz two outbursts with flickering superimposed cover the periods of high optical activity. Two outbursts are also visible at 43 and 37 GHz, but they are smoother and clearly delayed with respect to those at higher frequencies.

3. Swift-UVOT observations

The Ultraviolet/Optical Telescope (UVOT; Roming et al. 2005) onboard the Swift spacecraft (Gehrels et al. 2004) acquires data in the optical v, b, and u bands, as well as in the UV filters $uvw1$, $uvm2$, and $uvw2$ (Poole et al. 2008). In the period from 2008 May 27 to 2010 January 17, Swift pointed 173 times at 3C 454.3, acquiring data with the UVOT instrument 168 times. We reduced these data with the HEAsoft package version 6.10, with CALDB updated at the end of March 2010. Multiple exposures in the same filter at the same epoch were summed with `uvotimsum`, and then aperture photometry was performed with the task `uvotsource`. Source counts were extracted from a circular region with 5 arcsec radius, while background counts were estimated in two neighbouring source-free circular regions with 10 arcsec radii. In this way we obtained 147, 143, 165, 128, 126, and 120 photometric data in the $uvw2$, $uvm2$, $uvw1$, u, b, and v bands, respectively.

The UVOT light curves are shown in Fig. 3. The variability amplitude (maximum−minimum magnitude) decreases with increasing frequency: 1.94, 1.95, 1.88, 1.65, 1.48, and 1.46 mag going from the v to the $uvw2$ band. This confirms the trend already noticed for the optical data in Sect. 2 and extends it to the UV.

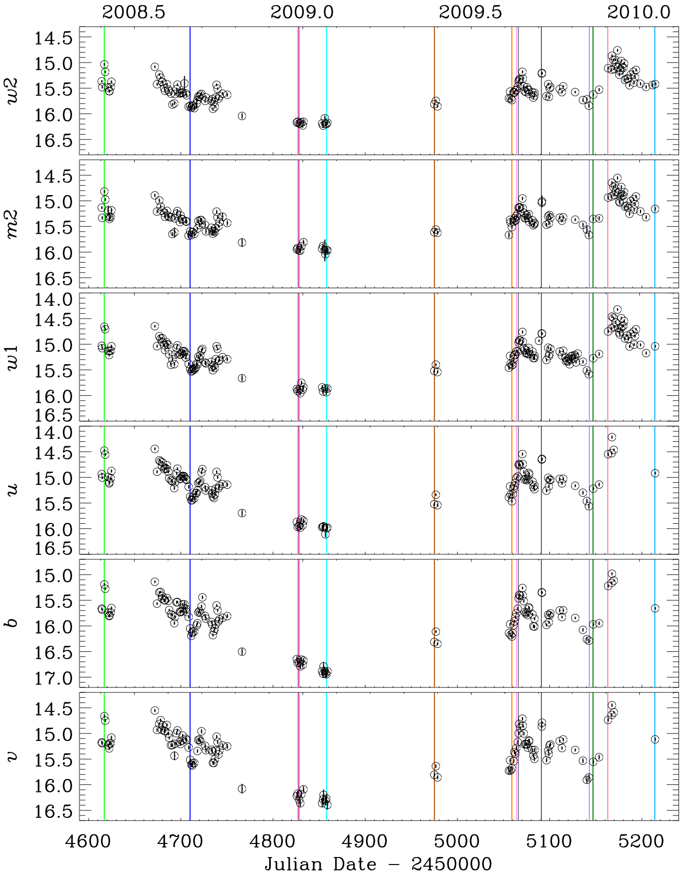

Fig. 3. Optical and UV light curves of 3C 454.3 in the 2008–2009 and 2009–2010 observing seasons. All data were acquired with the UVOT instrument onboard the Swift satellite. Vertical lines indicate the epochs selected for the calibration procedure.

The UVOT optical data are also reported in Fig. 1. In this case, shifts have been given to the UVOT magnitudes to match the ground-based U, B, and V data taken by the GASP-WEBT observers. We estimated mean offsets $U - u = 0.2$, $B - b = 0.1$, and $V - v = -0.05$, with an uncertainty of a few hundredths of mag. These values are the same as those derived for BL Lacertae by Raiteri et al. (2010). By considering that the average UVOT colour indices of 3C 454.3 are: $u - b \sim -0.7$ and $b - v \sim 0.5$, the UVOT photometric calibrations by Poole et al. (2008) would indicate $U - u \sim 0.2$, $B - b \sim 0$–0.02, and $V - v \sim 0.01$–0.02. While our offset in the u band agrees with their results, the offset we find in the other two bands is larger. This may partly depend on the uncertainties affecting the reference star photometry adopted for the calibration of the ground-based data. Moreover, we must also consider the different spectral shape of our source with respect to the Pickles stars and GRB models used by Poole et al. (2008) to make the UVOT calibrations. As a result, following Raiteri et al. (2010) we checked the calibrations for our source, calculating effective wavelengths, $\lambda_{\rm eff}$, and count rate to flux conversion factors, CF_Λ, by folding them with both the blazar spectrum and the effective areas of the UVOT filters. The same folding procedure was also applied to evaluate the amount of Galactic extinction for each band, A_Λ, starting from the Cardelli et al. (1989) laws. This is an important point, because the average extinction curve shows a bump at about 2175 Å, which makes the usual calculation of extinction at the filter $\lambda_{\rm eff}$ dangerous in the UV bands for very absorbed objects, as shown by Raiteri et al. (2010) for BL Lacertae. Galactic reddening towards 3C 454.3 is smaller than in the BL Lacertae case, so we expect that deviations from both the Poole et al. (2008) calibrations and the Galactic extinction evaluated at the filter $\lambda_{\rm eff}$ are milder. To verify this we selected a number of epochs where UVOT data were available in all filters and which represented different brightness levels of the source, and we built an average observed spectrum of 3C 454.3 (see Fig. 4, top panel). Then we fitted this mean spectrum with a log-cubic curve and used this fit in the folding procedure. We checked the stability of the results by iterating the procedure twice.

The new $\lambda_{\rm eff}$, CF_Λ, and A_Λ are reported in Table 1. For comparison, the corresponding "standard" values ($\lambda_{\rm eff}$ and CF_Λ by Poole et al. 2008; and A_Λ calculated at the $\lambda_{\rm eff}$ of Poole et al. 2008) are shown in brackets. We then obtained recalibrated flux densities from count rates using the new CF_Λ, and corrected for Galactic extinction according to the new A_Λ. In the bottom-left panel of Fig. 4 we show the resulting SEDs corresponding to the selected observing epochs, together with their average. This average is compared to that obtained from the average spectrum shown in the top panel after applying standard calibrations and de-reddening. The main differences are in the UV, where the recalibrated spectral shape is smoother.

As expected, there is a change in the spectral slope when going from bright to faint states, as the ratio between the optical and UV fluxes decreases, leading to the already noticed smaller flux-density variation at higher frequencies. This reveals the presence of another emission component, likely coming from the accretion disc and BLR. Indeed, BLR contributions to the source SED in the near-IR (Hα line), in the optical band (Mg II, Fe II, and Balmer lines), and in the UV (Lyα) have already

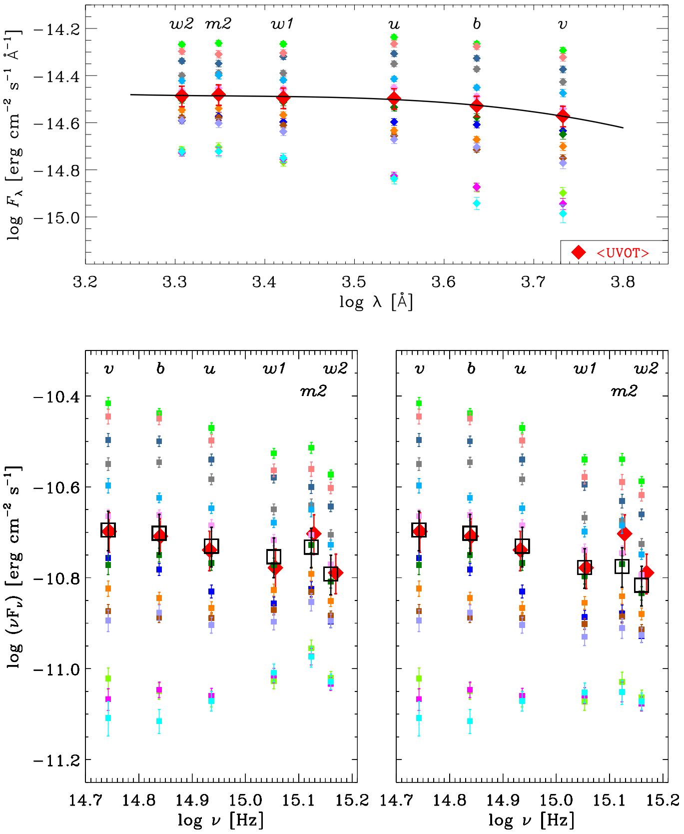

Fig. 4. *Top*: observed spectra of 3C 454.3 in the optical-UV band obtained from different epochs of UVOT observations analysed in this paper. Red diamonds refer to the mean UVOT observed spectrum. The solid line is the log-cubic fit used in the calibration procedure. *Bottom-left*: optical-UV SEDs of 3C 454.3 corresponding to the observed spectra shown in the top panel. Red diamonds are derived from the UVOT average spectra shown in the top panel by using standard prescriptions to obtain de-reddened flux densities. Black squares represent the mean UVOT SED after recalibration as explained in the text. *Bottom-right*: the same SEDs shown on the left, after correction for the emission lines contribution.

Table 1. Results of the UVOT recalibration procedure for 3C 454.3.

Filter	$\lambda_{\rm eff}$ Å	CF$_\Lambda$ 10^{-16} erg cm^{-2} s^{-1} Å^{-1}	A_Λ mag
v	5423 (5402)	2.61 (2.614)	0.36 (0.35)
b	4352 (4329)	1.47 (1.472)	0.47 (0.46)
u	3472 (3501)	1.65 (1.63)	0.57 (0.55)
*uvw*1	2652 (2634)	4.18 (4.00)	0.79 (0.73)
*uvm*2	2256 (2231)	8.42 (8.50)	0.99 (1.07)
*uvw*2	2074 (2030)	6.24 (6.2)	0.94 (1.02)

Notes. Values in brackets represent "standard" values, i.e. effective wavelengths $\lambda_{\rm eff}$ and count rate to flux conversion factors CF$_\Lambda$ from Poole et al. (2008), and Galactic extinction calculated from the Cardelli et al. (1989) laws at the $\lambda_{\rm eff}$ by Poole et al. (2008).

been recognised (Raiteri et al. 2007, 2008b; Benítez et al. 2010; Bonnoli et al. 2011). Subtraction of the Lyα flux would clarify to what extent a further contribution, possibly from the accretion disc, is needed. We used the publicly available UV spectrum acquired by the Galaxy Evolution Explorer[8] (GALEX) on 2008 September 30 to estimate the Lyα flux, finding $\sim 1.8 \times 10^{-14}$ erg cm^{-2} s^{-1}, about 30% lower than the value derived by Wills et al. (1995). By folding the line profile with the effective areas of the UV filters, we found contributions of 1.1, 3.1, and 1.2×10^{-16} erg cm^{-2} s^{-1} Å^{-1} in the *uvw*1, *uvm*2, and *uvw*2 bands, respectively. This means that in the *uvm*2 band the Lyα accounts for about 6% of the source flux density in the brightest state shown in Fig. 4, and for 17% in the faintest state. However, the Lyα line is not the only emission line to affect the UV spectrum of 3C 454.3. The *Hubble* Space Telescope (HST) spectra acquired in 1991 and analysed by Bahcall et al. (1993), Wills et al. (1995), and Evans & Koratkar (2004) also show prominent C IV and O VI + Lyβ lines, which are expected to mainly affect the flux in the *uvw*1 and *uvw*2 bands, respectively. We made a rough estimate of these further BLR contributions, finding that they are about one half of the Lyα ones. The bottom-right panel of Fig. 4 shows the source SEDs already displayed in the bottom-left panel, after correction for the emission line flux contribution. A UV excess still remains, likely indicating thermal emission from the accretion disc, as suggested by Raiteri et al. (2007, 2008b) and Bonnoli et al. (2011).

4. Spectral behaviour from the near-IR to the UV band

In the 2008–2009 observing season, near-IR monitoring in *J*, *H*, and *K* bands was performed at Campo Imperatore. L'Aquila earthquake that occurred on 2009 April 6 prevented the acquisition of data in the following season. Figure 5 shows four near-IR-to-UV SEDs obtained with simultaneous near-IR and optical GASP-WEBT data and the Swift-UVOT data treated as explained in the previous section, but without subtraction of the emission line contributions. To add information on the source behaviour at even fainter levels, we reconsidered the two SEDs corresponding to the *XMM-Newton* observations of July and December 2006, which were published by Raiteri et al. (2007). The corresponding near-IR and optical data were acquired by the WEBT collaboration, and they show the flux excess in the *J* band owing to the Hα emission line (see also Raiteri et al. 2008b) and the little bump in the optical, probably caused by Mg II, Fe II, and Balmer lines. The OM data shown in Fig. 6 of Raiteri et al. (2007) were treated in a standard way by converting magnitudes into fluxes according to the general method based on the Vega flux scale[9] and by correcting for Galactic extinction calculated from the Cardelli et al. (1989) law at the effective wavelength of the OM filters. We checked the reliability of those results by applying the same calibration procedure used in the previous section to check the UVOT calibrations.

Table 2 shows the results we obtained by folding the quantities of interest with both the source spectrum and the effective areas of the OM filters. The most noticeable difference between the new and the standard $\lambda_{\rm eff}$ is a blueshift in the *B* band, which makes the new value more like to the UVOT one. We also notice a 15% increase in the CF$_\Lambda$ in the *U* band over Vega and a 10% decrease in the Galactic extinction in the *UVW*2 band over the value we got from the Cardelli et al. (1989) law at the standard effective wavelength.

The main effect of the OM recalibration procedure is that the *U* points in Fig. 5 are shifted to a higher flux level than in Fig. 6 of Raiteri et al. (2007), confirming what we have already found for the UVOT data, i.e. that the satellite data are much brighter

---

[8] `http://www.galex.caltech.edu/`

[9] `http://xmm.esa.int/sas/current/watchout/Evergreen_tips_and_tricks/uvflux.shtml`

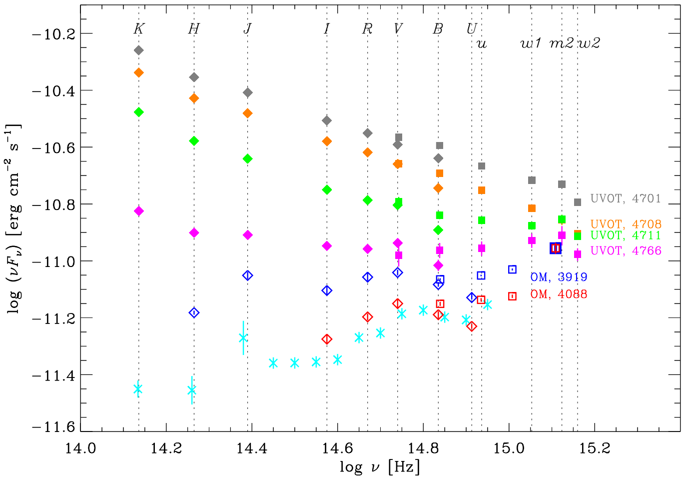

Fig. 5. SEDs of 3C 454.3 from the near-IR to the UV band at different brightness levels. The four SEDs plotted with filled symbols correspond to epochs of Swift observations: recalibrated UVOT data are displayed with squares, simultaneous optical and near-IR data from the GASP-WEBT with diamonds. The two SEDs shown with empty symbols correspond to the two *XMM-Newton* observations of July (blue) and December (red) 2006 (see Raiteri et al. 2007): recalibrated OM data are plotted with squares and WEBT data with diamonds. The epochs of satellite observations (JD − 2 450 000) are indicated on the right. Error bars only take measure errors into account. Cyan crosses represent observations by Neugebauer et al. (1979).

Table 2. Results of the OM recalibration procedure for 3C 454.3.

Filter	$\lambda_{\rm eff}$ Å	CF$_\Lambda$ 10^{-16} erg cm^{-2} s^{-1} Å^{-1}	A_Λ mag
V	5423 (5430)	2.53 (2.50)	0.36 (0.35)
B	4340 (4500)	1.35 (1.34)	0.47 (0.46)
U	3483 (3440)	1.96 (1.70)	0.56 (0.54)
*UVW*1	2945 (2910)	4.76 (4.86)	0.67 (0.65)
*UVM*2	2334 (2310)	21.8 (21.9)	0.96 (0.98)
*UVW*2	2146 (2120)	56.5 (58.8)	1.00 (1.10)

Notes. Values in brackets represent, respectively, "standard" effective wavelengths $\lambda_{\rm eff}$, count rate to flux conversion factors CF$_\Lambda$ based on Vega, and Galactic extinction calculated from the Cardelli et al. (1989) laws at the standard $\lambda_{\rm eff}$.

than the ground-based one in the *U* band. The recalibration of the OM data confirms the sharp rise of the SED in the UV when the source is in a faint state.

5. Swift-XRT observations

In the period from 2008 May 27 to 2010 January 17 (see Sect. 3) the XRT instrument onboard Swift (Burrows et al. 2005) performed 173 observations of 3C 454.3 in different observing modes. We processed the event files acquired in pointing mode, using the HEASoft package version 6.10 with CALDB updated as 2010 September 30. We considered the observations with exposure time longer than five minutes, including 111 observations in photon-counting (PC) mode and 59 in windowed-timing (WT) mode. The task `xrtpipeline` was run with standard filtering and screening criteria. For the PC mode, we selected event grades 0–12. Source counts were extracted from a 30 pixel circular region (~71 arcsec) centred on the source, and background counts were derived from a surrounding annular region with radii 110 and 160 pixels. When the count rate was greater than 0.5 counts/s, we punctured the source-extracting region, discarding the inner 3-pixel radius circle to correct for pile-up. The `xrtmkarf` task was used to generate ancillary response files (ARF), which account for different extraction regions, vignetting, and PSF corrections. The last in particular correct for the loss of counts caused by the central hole of the source extracting region in the pile-up case.

For the data acquired in WT mode, we selected event grades 0–2. We used the same circular region of 30 pixel radius centred on the source to extract the source counts, and a similar region shifted away from the source along the window to extract the background counts. When in the same observation the windows corresponding to different orbits overlapped with different position angles, we both created event files and extracted source and background counts separately for each orbit[10]. For each event file we then generated the exposure map with the task `xrtexpomap`, which was used to obtain the ARF for the corresponding source spectrum. Finally, we recombined the information from all the orbits of a single observation by summing the source spectra and the background spectra. The ARFs were summed by weighting them according to their orbit contribution to the total counts of the observation.

The task `grppha` was used to group the spectra and bin them to have more than 20 counts in each bin. These spectra were then analysed with the `xspec` task, version 12.6.0q. We applied an absorbed single power-law model, where absorption is modelled according to Wilms et al. (2000). Table 3 presents the result of the spectral analysis in the case where the hydrogen column is fixed to $N_{\rm H} = 1.34 \times 10^{21}$ cm^{-2}, as determined by the *Chandra* observations in 2005 (Villata et al. 2006). Column 1 gives the ObsID, Col. 2 the start time (UT), and Col. 3 the total exposure time, often distributed over several orbits. Column 4 gives the observing mode: an asterisk following "PC" means that the count rate was greater than 0.5 counts/s, and the data were thus corrected for pile-up, while a number following "WT" indicates how many misaligned windows were present in the total event file. Column 5 gives the photon index Γ, Col. 6 the 1 keV flux, Col. 7 the value of the reduced χ^2, while the number of degrees of freedom ν appears in brackets.

Some observations resulted in a low number of counts, and the corresponding χ^2/ν values were mostly small, indicating that the model is "over-fitting" the data. Indeed, the χ^2 statistic is not appropriate for a low number of counts, so that we refitted the spectra with either $\nu < 10$ or $\chi^2/\nu < 0.5$ adopting the Cash's C-statistic, which was developed to address this problem (Cash 1979; Nousek & Shue 1989). When in Col. 7 of Table 3 the label "Cash" appears, it means that the results of the spectral fit were obtained with the C-statistic. The photon index Γ ranges from 1.38 to 1.85, with an average value $\langle\Gamma\rangle = 1.59$, and a standard deviation $\sigma = 0.09$. However, the mean square uncertainty $\delta^2 = 0.18$ is greater than the variance σ^2, so that the mean fractional variation (Peterson 2001) $F_{\rm var} = \sqrt{\sigma^2 - \delta^2}/\langle\Gamma\rangle$ is not even real. This means that the spectral variations are dominated by noise and cannot be ascribed to real changes in the source spectrum. The lack of a trend of Γ with the source flux favours this interpretation.

6. Flux correlations

Figure 6 shows the multiwavelength behaviour of 3C 454.3 from May 2008 to January 2010. The top panel displays the

---

[10] We did not separate orbits if the misalignment was less than a few degrees.

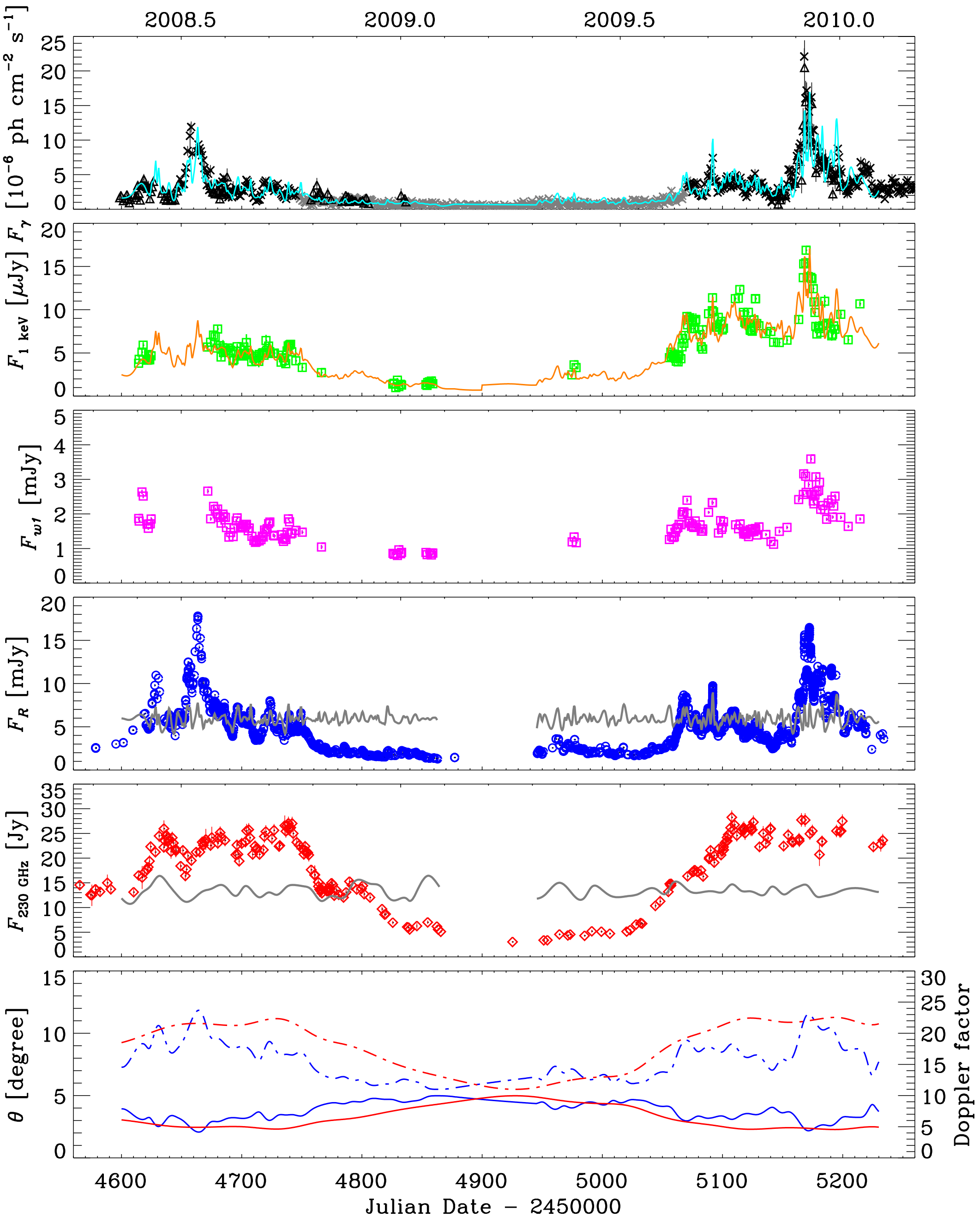

Fig. 6. Light curves of 3C 454.3 from May 2008 to January 2010 at different frequencies. The γ-ray data are 0.1–300 GeV fluxes; black triangles are from AGILE (Vercellone et al. 2010; Pacciani et al. 2010) and crosses from *Fermi* (the black ones from Abdo et al. 2009; and Ackermann et al. 2010, and the grey ones from the public light curve of the LAT monitored sources). The 1 keV flux densities are derived from Swift-XRT spectra fitted with an absorbed power law with $N_{\mathrm{H}} = 1.34\times10^{21}$ cm^{-2} (see Sect. 5 and Table 3). De-reddened UV flux densities in the $w1$ band are obtained as explained in Sect. 3. The optical R-band dereddened flux densities are derived from GASP data (see Sect. 2). The mm light curve is from the SMA. The cyan and orange curves superposed on the γ- and X-ray light curves, respectively, are obtained by combining cubic spline interpolations through the 1-day binned optical and the 7-day binned mm light curves as explained in the text. The *bottom panel* displays the evolution of the Doppler factors (dot-dashed lines) affecting the optical (blue) and mm (red) fluxes, and the viewing angles of the corresponding emitting regions (solid lines). Grey lines superposed on the optical and mm light curves represent intrinsic flux variations as would be observed under a constant Doppler factor $\delta = 18$.

0.1–300 GeV γ-ray light curve; the 2008–2009 AGILE data have already been published by Vercellone et al. (2010), and the 2009–2010 ones by Pacciani et al. (2010). *Fermi*-LAT data corresponding to the 2008 outburst are presented by Abdo et al. (2009), and those starting from August 2009 by Ackermann et al. (2010). For the period in between we downloaded the public *Fermi* light curve from HEASARC as 3C 454.3 is part of the *Fermi* LAT Monitored Source List[11]. The 1 keV flux densities plotted in the second panel are the result of the Swift-XRT spectral fitting with an absorbed power law with fixed absorption discussed in Sect. 5 and reported in Table 3. The

---

[11] `http://heasarc.gsfc.nasa.gov/W3Browse/fermi/fermilasp.html`

following ultraviolet (*uvw*1 band), optical (R band), and millimetric (230 GHz) light curves have already been shown in Figs. 1–3. We notice a rough correlation among the fluxes at all wavelengths, but the variability amplitude decreases from the higher to the lower frequencies, with the ultraviolet the only exception. Indeed, the maximum variation in the γ-ray flux is a factor ~214, while it is ~17 at 1 keV, ~14 in the optical R band, and ~9 at ~1 mm. The total change of the *uvw*1 flux density is only a factor ~5, and this is the consequence of the dilution of the variable synchrotron emission with the less variable disc and BLR radiation (see Sects. 3 and 4).

It is interesting to notice that the flux level reached by the optical light curve is similar in the two seasons; the same is true for the mm light curve, while in the X-ray and γ-ray bands there is a clear general flux increase in the second period. We miss information in the infrared, but can guess that the source behaviour would be intermediate between those in the optical and mm bands.

One possible interpretation of the observed long-term flux variations of 3C 454.3 at low frequencies (radio to UV) assumes that the jet is both inhomogeneous, with radiation of increasing wavelength being produced in progressively outer regions (e.g. Ghisellini & Maraschi 1989; Maraschi et al. 1992), and curved and that the alignment of the various emitting regions with the line of sight changes in time (Villata et al. 2006, 2007, 2009a). Because the Doppler factor $\delta = [\Gamma(1-\beta\cos\theta)]^{-1}$, where Γ is the bulk Lorentz factor of the jet plasma and $\beta = v/c$ its bulk velocity, depends on the viewing angle θ, the flux at a given wavelength will be Doppler-enhanced according to the orientation of the corresponding emitting zone. In the bottom panel of Fig. 6, we show the variation in the Doppler factors affecting the optical and mm fluxes under the hypothesis that their long-term trend is due to variations in the viewing angle alone and that the observed flux is proportional to δ^3 (see e.g. Urry & Padovani 1995; Villata & Raiteri 1999), so that $\delta(t) = \delta_{\rm min}[F(t)/F_{\rm min}]^{1/3}$. We set $\delta_{\rm min} = 11$, in the range of the values estimated by Abdo et al. (2009) and Ackermann et al. (2010) to avoid pair production, hence self-absorption, of γ-ray radiation. To reproduce the long-term trends we tentatively used cubic spline interpolations through the 7-d binned optical light curve and 30-d binned mm light curve[12]. In the bottom panel of Fig. 6 we also show the evolution of the corresponding viewing angles, obtained as $\theta(t) = \arccos\{[\Gamma\,\delta(\mathrm{t}) - 1]/[\sqrt{\Gamma^2-1}\,\delta(\mathrm{t})]\}$, where we put $\Gamma = 15.6$, in agreement with the value derived by long-term Very Long Baseline Interferometry (VLBI) monitoring (Jorstad et al. 2005). This produces maximum Doppler factors of ~23.7 for the optical and ~22.5 for the mm, and corresponding minimum viewing angles of about 2.1° and 2.3°, respectively, at the time of flux maxima. The minimum Doppler factor of 11, corresponding to a maximum angle of about 5.0°, was reached during the flux minima. The above picture would explain the long/mid-term flux variations (see also Villata et al. 2002, 2004), while the short-term flares (see below) would be due either to perturbations moving downstream in the jet or to a finer geometrical structure, as proposed for BL Lacertae by Larionov et al. (2010).

As mentioned in the Introduction, the high-energy emission is commonly believed to come from inverse-Comptonisation of low-energy radiation according to either an SSC or an EC process, or a combination of both. In an SSC scenario, the dependence of the synchrotron emissivity on the density of relativistic particles is linear, while the dependence of the self-Compton emissivity is quadratic. However, that the increase of the flux levels of the γ and X-ray light curves in the second observing season does not correspond to a rise of the optical and mm flux levels seems to rule out a variation in the electron density. The most straightward explanation is therefore that there has been a growth of the number of Comptonised seed photons, i.e. of the Comptonisation rate.

We investigate the matter in an SSC framework and we roughly divide the emitting jet in three zones, where radiation at different frequencies is produced through the synchrotron process: the UV to near-IR region, which we will call the "optical" region, the IR region, and the mm region[13]. We assume that the variation in time of the number of both synchrotron (seed) photons and target electrons in the various zones is represented by the R-band light in the first region, by a linear combination of the R-band and mm light curves in the second region, and by the mm flux density variations in the third region. We therefore try to fit the γ and X-ray light curves in Fig. 6 with the following general expression:

$$[s_R\,F_R(t)/\delta^3_R(t) + s_{\rm mm}\,F_{\rm mm}(t)/\delta^3_{\rm mm}(t)] \times [e_R\,F_R(t) + e_{\rm mm}\,F_{\rm mm}(t)]$$

where the first factor refers to the seed photons in the jet rest frame, the second factor to the Comptonising electrons, $F_R(t)$ and $F_{\rm mm}(t)$ represent cubic spline interpolations through the 1-d binned R-band and 7-d binned mm light curves, respectively, $\delta_R(t)$ and $\delta_{\rm mm}(t)$ are the Doppler factors affecting the optical and mm emissions, respectively, which are plotted in the bottom panel of Fig. 6, and $s_R, s_{\rm mm}, e_R, e_{\rm mm}$ are coefficients that regulate the relative contributions of the jet zones. The functions $F'_R(t) = F_R(t)/\delta^3_R(t)$ and $F'_{\rm mm}(t) = F_{\rm mm}(t)/\delta^3_{\rm mm}(t)$ represent the intrinsic optical and mm flux density changes, respectively, since δ^{-3} corrects for the variability due to the Doppler boosting. To better clarify this point, we superposed, on the optical and mm light curves in Fig. 6, those intrinsic changes that would be observed in case of a constant Doppler factor $\delta = 18$, i.e. if there were no viewing angle variations. As one can see, ascribing the long-term trends to viewing angle variations on the chosen time scales (one week for the optical, one month for the mm) reveals intrinsic variations of similar amplitude, which in turn supports the initial assumption.

The fit to the γ-ray light curve shown in the top panel of Fig. 6 is obtained by setting $s_{\rm mm} = e_{\rm mm} = 0$, suggesting that the γ-ray emission comes from the Comptonisation of synchrotron optical photons in the optical emitting region. However, due to the photon's mean free path before upscattering and to the fact that the synchrotron radiation is relativistically beamed forward, the bulk of the γ-ray radiation is expected to come from a region slightly downstream from the region responsible for the bulk of the optical emission. To fit the X-ray light curve, we set $s_R = e_R$ and $s_{\rm mm} = e_{\rm mm}$, meaning that the X-ray emission is obtained by upscattering of IR photons on their parent relativistic electrons. Also in this case we can imagine that the bulk of the X-ray radiation is produced a bit downstream from the bulk of the IR radiation.

The increase in the γ and X-ray flux levels from the first to the second observing season can thus be explained as a growth in the number of seed photons that are Comptonised. In particular, to explain the higher γ flux in the second season, we need to increase the number of Comptonising interactions by about 60%, while we need to increase it by a factor 1.6–1.8 to explain the

---

[12] The mm emitting region is expected to be much wider than the optical one, so that its variability time scales would be longer.

[13] Indeed, in our inhomogeneous jet model the synchrotron emission at each frequency mainly comes from the jet region where that frequency is close to self absorption.

higher X-ray flux. This may be due to a variable misalignment between the zone responsible for the bulk of the synchrotron emission and the one responsible for the bulk of the respective inverse-Compton one. In the second observing season, the regions would be better aligned, so that more seed photons can enter the corresponding Comptonisation zone.

In summary, we imagine a scenario where the variation in the angle between our line of sight and the optical emitting region in the 2008–2009 observing season is similar to the variation in the following 2009–2010 season, implying similar flux density levels. The same is true for the mm region. At the same time, the γ and X-ray production zones become more aligned with the optical and IR regions in the second period, explaining the increased γ and X-ray flux levels.

6.1. Short-term correlation between the optical and γ-ray fluxes

The correlation between the γ-ray and optical fluxes of 3C 454.3 has been analysed in a number of papers including AGILE or *Fermi* data. Using AGILE and WEBT data, Vercellone et al. (2009) find a mild correlation with no evident time delay in November 2007, while the increased optical activity in December allowed Donnarumma et al. (2009) to constrain the γ-optical time lag to $-0.6^{+0.7}_{-0.5}$ d, indicating that the γ-ray flux variations follow the optical ones by ~0–1 d, even if a very fast γ and optical flare on December 12 seemed to constrain the delay within 12 h. When considering 18 months of AGILE and GASP-WEBT observations (2007 July–2009 January), Vercellone et al. (2010) found a time lag of $-0.4^{+0.6}_{-0.8}$ d of the γ-ray variations after the optical ones, consistent with the earlier results. The cross-correlation study performed by Bonning et al. (2009) on γ-ray data from *Fermi* and optical/IR data from SMARTS in 2008 found no detectable lag between IR/optical and γ-ray fluxes.

Figure 7 shows an enlargement of the γ and optical light curves of Fig. 6 around the brightest phase of the 2008 outburst. The γ-ray flare appears double-peaked, the flux of the first maximum being 27% higher than that of the second one. The shape of the optical flare seems more complex, but we notice that there is an optical minor peak corresponding to the first γ maximum, just before or simultaneous to it, and there is a major optical peak just before or simultaneous to the second γ peak. It is not clear whether there are really more optical events than γ ones, or if other γ peaks are hidden by insufficient sampling and precision. Moreover, it is not easy to understand why a minor (major) optical flare corresponds to a major (minor) event at γ energies.

The period of most intense activity in late 2009 is shown in Fig. 8. We can recognise some features similar to those noticed in the light curves of mid 2008. The dense optical monitoring performed by the GASP collaboration allowed us to detect a sharp peak on JD = 2 455 168, simultaneous to the major γ-ray one. Then, a second major fast optical flare at JD = 2 455 172 found the γ-ray flux at a much lower level, possibly in between two little γ bumps. We again notice a difference in the flux ratios: the second optical peak is brighter than the first one, whereas the opposite is true in γ-rays. Moreover, a well-sampled optical minimum is visible at JD = 2 455 176, while the minimum is reached 1–2 days later at γ frequencies. Finally, the optical flares peaking at JD = 2 455 183 and JD = 2 455 190 have no evident γ-ray counterparts.

In summary, when inspecting the γ-optical correlation on short time scales, sometimes the optical and γ flux variations are simultaneous, whereas in other cases the latter seem to be lacking or to possibly be delayed.

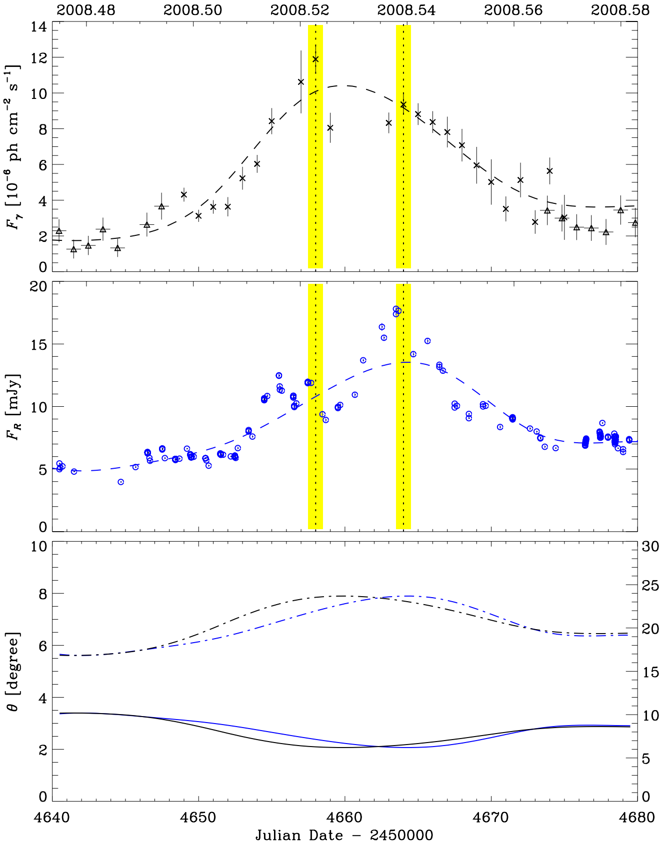

Fig. 7. Flux variations of 3C 454.3 at γ-ray (*top*) and optical (*middle*) frequencies in mid 2008. The γ-ray light curve is built with *Fermi* data (crosses) from Abdo et al. (2009) and AGILE data (triangles) from Vercellone et al. (2010). Vertical dotted lines indicate the position of the two γ peaks, the yellow stripes highlighting the data integration interval. Cubic spline interpolations through the 7-day binned optical (blue dashed line) and γ (black dashed line) light curves are also shown. They represent the variations due to geometrical changes. The evolution of the Doppler factor δ (dot-dashed lines) and viewing angle θ (solid lines) is shown in the bottom panel for both the γ-ray (black) and optical (blue) bands.

In the geometrical scenario proposed above to explain the long-term flux variations of the optical and mm light curves, as well as the increased γ and X-ray fluxes in 2009–2010, a slight misalignment between the regions responsible for the production of the optical and γ-ray radiations can also account for the variation in the γ/optical flux ratio. In the bottom panels of Figs. 7 and 8 we show the evolution of the Doppler factors δ and viewing angles θ affecting the optical and γ fluxes in the considered periods. The trends of the optical δ and θ have already been presented in the bottom panel of Fig. 6. To obtain the γ-ray ones we used cubic spline interpolations through the 7-d binned *Fermi* light curve and rescaled it to the optical one to take into account that we are comparing fluxes deriving from different processes. We therefore constructed a new γ-ray spline as $F_{\rm res} = a F^b$, which has the same flux maximum and minimum as the optical one. We got $a = 3.53$ and $b = 0.57$ in the period shown in Fig. 7, while $a = 1.70$ and $b = 0.73$ in the period plotted in Fig. 8[14]. In both periods one can see that the γ-emitting region acquires the minimum θ, corresponding to the maximum δ, slightly before

---

[14] This means that in the considered periods the total long-term variation in the γ flux is less than quadratic with respect to the optical one, as expected, because the quadratic dependence of the intrinsic fluxes is "diluted" by the Doppler factor variation.

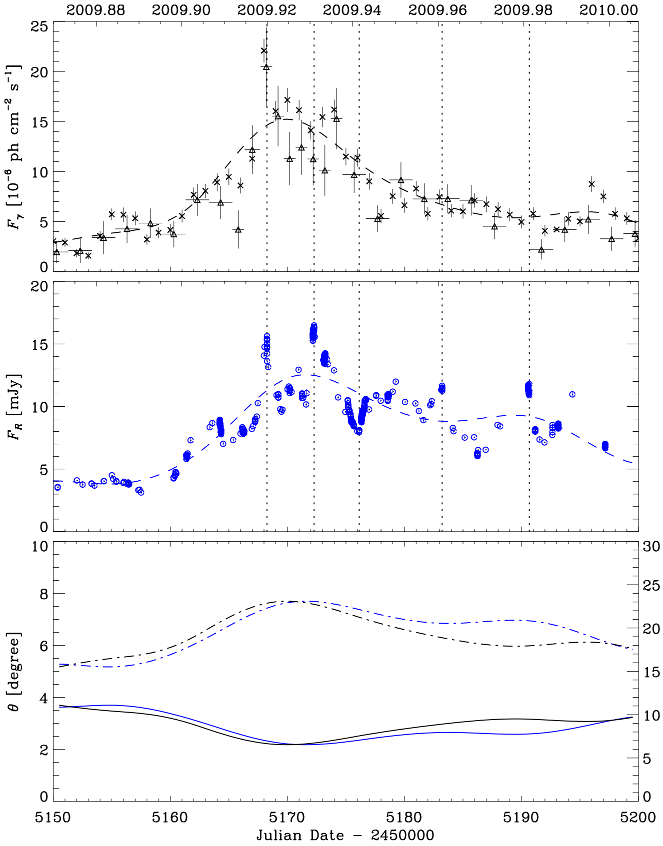

Fig. 8. Flux variations of 3C 454.3 at γ-ray (*top*) and optical (*middle*) frequencies in late 2009. The γ-ray light curve is built with *Fermi* data (crosses) from Ackermann et al. (2010) and AGILE data (triangles) from Pacciani et al. (2010). Vertical dotted lines indicate remarkable optical events. Cubic spline interpolations through the 7-day binned optical (blue dashed line) and γ (black dashed line) light curves are also shown. They represent the variations due to geometrical changes. The evolution of the Doppler factor δ (dot-dashed lines) and viewing angle θ (solid lines) is shown in the bottom panel for both the γ-ray (black) and optical (blue) bands.

than the optical zone. We suggest that in both periods, because of the different orientation of the emitting regions, the γ-ray flux was more relativistically boosted than the optical one at the time of the first γ peak, while the opposite occurred at the time of the second peak. Moreover, we can see that, in the rising part of the 2009 outburst, the two regions are better aligned, yielding more comparable optical and γ flares than in the rising part of the 2008 outburst. The maximum misalignment between the optical and γ emitting regions is quite small: $\sim 0.4°$ in mid 2008 and $\sim 0.6°$ in late 2009.

6.2. Short-term correlation between the X-ray and optical/γ fluxes

The X-ray light curve is less sampled than the γ-ray one, so that a detailed analysis of correlation like the one performed in the previous section is not possible. We thus investigate the optical-X correlation by analysing the entire long-term light curves shown in Fig. 6 by means of the discrete correlation function (DCF; Edelson & Krolik 1988; Hufnagel & Bregman 1992), which was specifically designed to study unevenly sampled data sets. In Fig. 9 we show the DCF obtained by cross-correlating the 1 keV with the R-band flux densities. Both light curves have previously been binned over 12 h, while the DCF bin was set to two days. The curve peaks at a time lag τ between -2 and 0 d, with a DCF value of 0.62, which indicates mild correlation, and flux variations in the optical band leading or being simultaneous to those in the X-ray one. In general, a more precise measure of the time lag can be obtained by calculating the centroid of the DCF, $\tau_{\rm c} = (\sum_i \tau_i {\rm DCF}_i)/(\sum_i {\rm DCF}_i)$, where sums run over the points which have a DCF value close to the peak one. In our case the calculation of the centroid using all points with DCF $> 0.8\,{\rm DCF}_{\rm peak}$ (6 points) yields $\tau_{\rm c} = -1.0$ d, i.e. an X-ray lag of 1 d. The same result is obtained by lowering the threshold for the centroid calculation to 0.75 and 0.70 of the ${\rm DCF}_{\rm peak}$ (8 points). To estimate the uncertainty on this time lag, we performed Monte Carlo simulations following the technique known as "flux redistribution/random subset selection" (FR/RSS; Peterson et al. 1998; see also Raiteri et al. 2003), which allows testing the influence of both sampling and errors on the results. We randomly selected subsets of the X-ray and optical light curves, discarding redundant points, and adding to the fluxes random Gaussian deviates constrained by the flux errors. The X-ray and optical subsets are then cross-correlated and the resulting DCF centroids stored. A measure of the lag uncertainty can then be derived from the centroid distribution, by considering the range of $\tau_{\rm c}$ values containing 68.27% of the realisations. The inset in Fig. 9 displays the $\tau_{\rm c}$ distribution obtained from 1000 Monte Carlo realisations: $\tau_{\rm c}$ is in the range -2–0 d in 71% of cases ($\gtrsim 1\sigma$). This allows us to conclude in a more precise way that the time lag of the X-ray flux variations after the optical ones is $\tau = 1.0 \pm 1.0$ d.

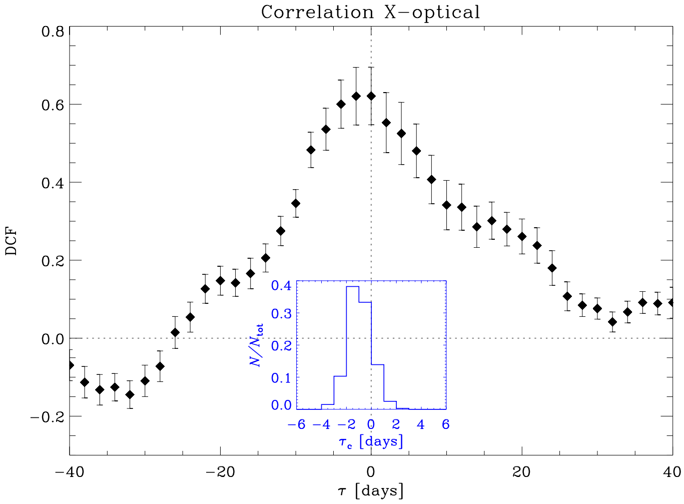

Fig. 9. Discrete correlation function (DCF) between the 1 keV flux densities from XRT and the GASP R-band flux densities. The inset shows the results of 1000 Monte Carlo simulations.

The finding of a time delay of the X-ray variations after the optical ones agrees with the picture proposed above, where the X-ray radiation is produced in the IR region, downstream of the optical one. In the proposed scenario we would also expect the X-ray emission to be slightly delayed with respect to the γ-ray one, which is supposed to be very close to the optical one. Cross-correlation of the γ-ray light curve with the X-ray one, with the same choice of binning parameters as in the X-ray/optical case, yields a highly significant peak (${\rm DCF}_{\rm peak} \sim 1$) at zero time lag, while $\tau_{\rm c} = 1.0$ d. The result of the Monte Carlo method described above is $\tau = 0.5 \pm 1.0$ d, confirming a possible slight delay in the X-ray flux variations.

7. Conclusions

In this paper we have presented multifrequency observations of 3C 454.3 from April 2008 to March 2010. Radio-to-optical data are mainly from the GASP-WEBT, and UV and X-ray data are from Swift and γ-ray data from AGILE and *Fermi*. In these two observing seasons, the source showed prominent outbursts at frequencies greater than 8 GHz, with rapid flares superposed in the optical-to-γ light curves.

We have reanalysed the question of the nature of the optical-UV emission, deriving more accurate calibrations for both the UVOT instrument onboard Swift and the OM detector onboard *XMM-Newton*, and estimating the contribution of the emission lines (mainly Lyα) in the UV. We confirmed that the observed decrease of the variability amplitude with increasing frequency from the near-IR to the UV band is due to the contribution of radiation from both the BLR and the accretion disc. The long-term flux variations from the optical to the γ-ray frequencies appear roughly correlated. The mm flux remained high during the whole optical flaring period.

By comparing the multiwavelength behaviour in the 2008–2009 and 2009–2010 observing seasons, we noticed that the optical flux reached nearly the same levels (i.e. minimum and maximum brightness) in both seasons. The same thing occurred in the mm band, whereas the γ-ray and X-ray flux levels increased in the second period.

We interpreted the observations in terms of an inhomogeneous jet model, where synchrotron radiation of increasing wavelength is produced in progressively larger regions farther away from the emitting jet apex. The jet is supposed to be a curved (possibly in a helical shape) and flexible (maybe rotating) structure, where different emitting zones have different alignments with the line of sight, and their viewing angle can change in time. A similar model has been adopted to explain the multiwavelength behaviour of Mkn 501 (Villata & Raiteri 1999), S4 0954+65 (Raiteri et al. 1999), BL Lacertae (Villata et al. 2002, 2004, 2009b; Raiteri et al. 2009, 2010; Larionov et al. 2010), AO 0235+164 (Ostorero et al. 2004), along with 3C 454.3 (Villata et al. 2006, 2007, 2009a).

We assumed that the long-term flux density variations, with a tentative time scale of one week in the optical and of one month in the mm band, are due to changes of the viewing angles of the corresponding emitting regions, while variability on shorter time scales can be ascribed either to intrinsic flaring activity or to a finer geometrical structure (as suggested by Larionov et al. 2010, for BL Lacertae). Then, under the further assumption that the γ and X-ray emissions are produced by inverse-Compton scattering of synchrotron photons and that the behaviour of the IR light curve is intermediate between the optical and mm ones, we combined the optical and mm fluxes to fit the γ and X-ray light curves. In this scenario the multiwavelength observations presented in this paper suggest that the γ-ray radiation comes from inverse-Comptonisation of "optical" (actually UV to-near-IR) synchrotron photons produced in the inner emitting jet region by their parent relativistic electrons (SSC process). However, depending on the mean free path before upscattering, the bulk of the γ-ray radiation is produced in a region slightly downstream of the one responsible for the bulk of the optical emission. The jet curvature then implies that the γ and optical regions are slightly misaligned. A reduction of this misalignment, allowing more optical seed photons to enter the Comptonisation zone, could thus be at the origin of the γ-ray flux increase in 2009–2010. Moreover, the variation in the γ/optical flux ratio during the outburst peaks of mid 2008 and late 2009 can be explained by the fact that the γ zone acquires the minimum viewing angle, hence the maximum Doppler boosting, some days before the optical zone.

The X-ray light curve is not as well sampled as the optical and γ-ray ones, which makes a detailed analysis more difficult. However, the above-mentioned fit suggests that the X-ray radiation comes from a downstream region, where relativistic electrons produce and upscatter synchrotron IR photons (SSC process). The rise in the X-ray flux levels in the 2009–2010 season would then be explained similarly to the case of the γ flux, with a better alignment between the zones responsible for the bulk of the synchrotron and inverse-Compton emissions. The mean delay of about 1 d of the X-ray flux variations after the optical ones and of about 0.5 d after the γ-ray ones, found by cross-correlation analysis, are consistent with this picture.

Acknowledgements. C.M.R. is grateful to Stefania Rasetti from the Torino Observatory Computer Centre for her assistance. We thank the *Fermi*-LAT team for providing *Fermi* data. We acknowledge the use of public data from the Swift data archive. We acknowledge financial contribution from the agreement ASI-INAF I/009/10/0. St.-Petersburg University team acknowledges support from Russian RFBR foundation via grant 09-02-00092. Abastumani Observatory team acknowledges financial support by the Georgian National Science Foundation through grant GNSF/ST08/4-404. The Metsähovi team acknowledges the support from the Academy of Finland to our observing projects (numbers 212656, 210338, 121148, and others). The University of Michigan team acknowledges financial support through the NASA *Fermi* grants NNX09AU16G, NNX10AP16G, and NSF grant AST-0607523. The operation of UMRAO is funded by the University of Michigan. This paper is partly based on observations carried out at the German-Spanish Calar Alto Observatory, which is jointly operated by the MPIA and the IAA-CSIC. Acquisition of the MAPCAT data is supported in part by MICIIN (Spain) grant and AYA2010-14844, and by CEIC (Andalucía) grant P09-FQM-4784. Partly based on observations with the Medicina and Noto telescopes operated by INAF – Istituto di Radioastronomia. This research has made use of NASA's Astrophysics Data System and of the XRT Data Analysis Software (XRTDAS) developed under the responsibility of the ASI Science Data Center (ASDC), Italy. This research has made use of data from the MOJAVE database that is maintained by the MOJAVE team (Lister et al. 2009). The Submillimeter Array is a joint project between the Smithsonian Astrophysical Observatory and the Academia Sinica Institute of Astronomy and Astrophysics and is funded by the Smithsonian Institution and the Academia Sinica. The research at Boston U. was supported by NSF grant AST-0907893 and NASA *Fermi* GI grants NNX08AV65G, NNX08AV61G, and NNX09AT99G. The PRISM camera at Lowell Observatory was developed by K. Janes et al. at BU and Lowell Observatory, with funding from the NSF, BU, and Lowell Observatory.

References

Abdo, A. A., Ackermann, M., Ajello, M., et al. 2009, ApJ, 699, 817
Abdo, A. A., Ackermann, M., Ajello, M., et al. 2010, ApJ, 716, 835
Abdo, A. A., Ackermann, M., Ajello, M., et al. 2011, ApJ, 733, L26
Ackermann, M., Ajello, M., Baldini, L., et al. 2010, ApJ, 721, 1383
Anderhub, H., Antonelli, L. A., Antoranz, P., et al. 2009, A&A, 498, 83
Bahcall, J. N., Bergeron, J., Boksenberg, A., et al. 1993, ApJS, 87, 1
Benítez, E., Chavushyan, V. H., Raiteri, C. M., et al. 2010, in Accretion and Ejection in AGN: a Global View, ed. L. Maraschi, G. Ghisellini, R. Della Ceca, & F. Tavecchio, ASP Conf. Ser., 427, 291
Bessell, M. S., Castelli, F., & Plez, B. 1998, A&A, 333, 231
Bonning, E. W., Bailyn, C., Urry, C. M., et al. 2009, ApJ, 697, L81
Bonnoli, G., Ghisellini, G., Foschini, L., Tavecchio, F., & Ghirlanda, G. 2011, MNRAS, 410, 368
Burrows, D. N., Hill, J. E., Nousek, J. A., et al. 2005, Space Sci. Rev., 120, 165
Cardelli, J. A., Clayton, G. C., & Mathis, J. S. 1989, ApJ, 345, 245
Cash, W. 1979, ApJ, 228, 939
Dermer, C. D., Finke, J. D., Krug, H., & Böttcher, M. 2009, ApJ, 692, 32
Donnarumma, I., Pucella, G., Vittorini, V., et al. 2009, ApJ, 707, 1115
Edelson, R. A., & Krolik, J. H. 1988, ApJ, 333, 646
Evans, I. N., & Koratkar, A. P. 2004, ApJS, 150, 73
Finke, J. D., & Dermer, C. D. 2010, ApJ, 714, L303
Foschini, L., Tagliaferri, G., Ghisellini, G., et al. 2010, MNRAS, 408, 448
Fuhrmann, L., Cucchiara, A., Marchili, N., et al. 2006, A&A, 445, L1
Gehrels, N., Chincarini, G., Giommi, P., et al. 2004, ApJ, 611, 1005

Ghisellini, G., & Maraschi, L. 1989, ApJ, 340, 181
Ghisellini, G., Foschini, L., Tavecchio, F., & Pian, E. 2007, MNRAS, 382, L82
Giommi, P., Blustin, A. J., Capalbi, M., et al. 2006, A&A, 456, 911
Gurwell, M. A., Peck, A. B., Hostler, S. R., Darrah, M. R., & Katz, C. A. 2007, in From Z-Machines to ALMA: (Sub)Millimeter Spectroscopy of Galaxies, ed. A. J. Baker, J. Glenn, A. I. Harris, J. G. Mangum, & M. S. Yun, ASP Conf. Ser., 375, 234
Hufnagel, B. R., & Bregman, J. N. 1992, ApJ, 386, 473
Jorstad, S. G., Marscher, A. P., Lister, M. L., et al. 2005, AJ, 130, 1418
Jorstad, S. G., Marscher, A. P., Larionov, V. M., et al. 2010, ApJ, 715, 362
Larionov, V. M., Villata, M., & Raiteri, C. M. 2010, A&A, 510, A93
Lister, M. L., Aller, H. D., Aller, M. F., et al. 2009, AJ, 137, 3718
Maraschi, L., Ghisellini, G., & Celotti, A. 1992, ApJ, 397, L5
Neugebauer, G., Oke, J. B., Becklin, E. E., & Matthews, K. 1979, ApJ, 230, 79
Nousek, J. A., & Shue, D. R. 1989, ApJ, 342, 1207
Ogle, P. M., Wehrle, A. E., Balonek, T., & Gurwell, M. A. 2011, ApJS, 195, 19
Ostorero, L., Villata, M., & Raiteri, C. M. 2004, A&A, 419, 913
Pacciani, L., Vittorini, V., Tavani, M., et al. 2010, ApJ, 716, L170
Peterson, B. M. 2001, in Advanced Lectures on the Starburst-AGN Connection, ed. I. Aretxaga, D. Kunth, & R. Mújica (Singapore: World Scientific), 3
Peterson, B. M., Wanders, I., Horne, K., et al. 1998, PASP, 110, 660
Pian, E., Foschini, L., Beckmann, V., et al. 2006, A&A, 449, L21
Poole, T. S., Breeveld, A. A., Page, M. J., et al. 2008, MNRAS, 383, 627
Raiteri, C. M., Villata, M., Lanteri, L., Cavallone, M., & Sobrito, G. 1998, A&AS, 130, 495
Raiteri, C. M., Villata, M., Tosti, G., et al. 1999, A&A, 352, 19
Raiteri, C. M., Villata, M., Tosti, G., et al. 2003, A&A, 402, 151
Raiteri, C. M., Villata, M., Larionov, V. M., et al. 2007, A&A, 473, 819
Raiteri, C. M., Villata, M., Chen, W. P., et al. 2008a, A&A, 485, L17
Raiteri, C. M., Villata, M., Larionov, V. M., et al. 2008b, A&A, 491, 755
Raiteri, C. M., Villata, M., Capetti, A., et al. 2009, A&A, 507, 769
Raiteri, C. M., Villata, M., Bruschini, L., & Capetti, A. 2010, A&A, 524, A43
Roming, P. W. A., Kennedy, T. E., Mason, K. O., et al. 2005, Space Sci. Rev., 120, 95
Sasada, M., Uemura, M., Arai, A., et al. 2010, PASJ, 62, 645
Sikora, M., Moderski, R., & Madejski, G. M. 2008, ApJ, 675, 71
Striani, E., Vercellone, S., Tavani, M., et al. 2010, ApJ, 718, 455
Tavecchio, F., Ghisellini, G., Bonnoli, G., & Ghirlanda, G. 2010, MNRAS, 405, L94
Urry, C. M., & Padovani, P. 1995, PASP, 107, 803
Vercellone, S., Chen, A. W., Giuliani, A., et al. 2008, ApJ, 676, L13
Vercellone, S., Chen, A. W., Vittorini, V., et al. 2009, ApJ, 690, 1018
Vercellone, S., D'Ammando, F., Vittorini, V., et al. 2010, ApJ, 712, 405
Villata, M., & Raiteri, C. M. 1999, A&A, 347, 30
Villata, M., Raiteri, C. M., Kurtanidze, O. M., et al. 2002, A&A, 390, 407
Villata, M., Raiteri, C. M., Kurtanidze, O. M., et al. 2004, A&A, 421, 103
Villata, M., Raiteri, C. M., Balonek, T. J., et al. 2006, A&A, 453, 817
Villata, M., Raiteri, C. M., Aller, M. F., et al. 2007, A&A, 464, L5
Villata, M., Raiteri, C. M., Larionov, V. M., et al. 2008, A&A, 481, L79
Villata, M., Raiteri, C. M., Gurwell, M. A., et al. 2009a, A&A, 504, L9
Villata, M., Raiteri, C. M., Larionov, V. M., et al. 2009b, A&A, 501, 455
Wills, B. J., Thompson, K. L., Han, M., et al. 1995, ApJ, 447, 139
Wilms, J., Allen, A., & McCray, R. 2000, ApJ, 542, 914

---

[1] INAF, Osservatorio Astronomico di Torino, Italy
e-mail: `raiteri@oato.inaf.it`
[2] Department of Astronomy, University of Michigan, MI, USA
[3] Harvard-Smithsonian Center for Astrophysics, Cambridge, MA, USA
[4] Abastumani Observatory, Mt. Kanobili, Abastumani, Georgia
[5] Aalto University Metsähovi Radio Observatory, Kylmälä, Finland
[6] Astron. Inst., St.-Petersburg State Univ., Russia
[7] Pulkovo Observatory, St.-Petersburg, Russia
[8] Isaac Newton Institute of Chile, St.-Petersburg Branch, Russia
[9] INAF-IASF Palermo, Italy
[10] Instituto de Astrofísica de Andalucía, CSIC, Granada, Spain
[11] Institute for Astrophysical Research, Boston University, MA, USA
[12] Max-Planck-Institut für Radioastronomie, Bonn, Germany
[13] Instituto de Astronomía, Universidad Nacional Autónoma de México, Mexico
[14] Tuorla Observatory, Univ. of Turku, Piikkiö, Finland
[15] Astrophysical Inst., Department of Physics and Astronomy, Ohio Univ., Athens OH, USA
[16] INAF, Osservatorio Astrofisico di Catania, Italy
[17] Osservatorio Astronomico della Regione Autonoma Valle d'Aosta, Italy
[18] EPT Observatories, Tijarafe, La Palma, Spain
[19] INAF, TNG Fundación Galileo Galilei, La Palma, Spain
[20] Institut de Ciències de l'Espai (CSIC-IEEC), Spain
[21] Agrupació Astronòmica de Sabadell, Spain
[22] Graduate Institute of Astronomy, National Central University, Taiwan
[23] ZAH, Landessternwarte Heidelberg-Königstuhl, Germany
[24] Lulin Observatory, National Central University, Taiwan
[25] School of Cosmic Physics, Dublin Institute For Advanced Studies, Ireland
[26] Department of Physics, National Taiwan University, Taipei, Taiwan
[27] Circolo Astrofili Talmassons, Italy
[28] Department of Physics, Purdue University, West Lafayette, IN, USA
[29] Finnish Centre for Astronomy with ESO (FINCA), University of Turku, Piikkiö, Finland
[30] Facultad de Ciencias Espaciales, Univ. Nacional Autonoma de Honduras, Tegucigalpa M.D.C., Honduras
[31] Department of Physics, Univ. of Colorado Denver, CO, USA
[32] Center for Research and Exploration in Space Science and Technology, NASA/GSFC, Greenbelt, MD, USA
[33] Galaxy View Observatory, Sequim, Washington, USA
[34] Lowell Observatory, Flagstaff, AZ, USA
[35] Radio Astronomy Laboratory of Crimean Astrophysical Observatory, Ukraine

Pages 14 to 16 are available in the electronic edition of the journal at http://www.aanda.org

Table 3. Results of the analysis of the XRT observations.

ObsID	START	JD $-2\,450\,000$	Exp [s]	Mode	Γ	$F_{1\ \mathrm{keV}}$ [μJy]	$\chi^2/\nu\,(\nu)$
00031216001	2008-05-27 16:45:01	4614.19793	3982	PC*	1.54 ± 0.07	3.81 ± 0.22	0.95 (65)
00031216002	2008-05-28 04:08:01	4614.67223	2023	PC*	1.57 ± 0.08	4.26 ± 0.29	1.16 (45)
00031216003	2008-05-30 12:18:00	4617.01250	2144	PC*	1.56 ± 0.07	5.09 ± 0.33	0.99 (53)
00031216004	2008-05-31 12:22:01	4618.01529	2144	PC*	1.47 ± 0.06	5.90 ± 0.35	1.12 (68)
00031216005	2008-06-03 18:45:10	4621.28137	1995	PC*	1.57 ± 0.10	4.16 ± 0.37	1.19 (32)
00031216006	2008-06-04 18:50:57	4622.28538	1995	PC*	1.56 ± 0.09	4.20 ± 0.31	0.68 (40)
00031216007	2008-06-05 01:35:00	4622.56597	2137	PC*	1.59 ± 0.08	4.82 ± 0.33	0.66 (46)
00031216008	2008-06-06 00:19:01	4623.51321	2079	PC*	1.59 ± 0.09	4.21 ± 0.31	0.71 (42)
00031216009	2008-06-07 02:03:01	4624.58543	1807	PC*	1.59 ± 0.09	4.66 ± 0.35	1.29 (41)
00031216010	2008-07-24 00:10:01	4671.50696	1952	PC*	1.55 ± 0.07	5.68 ± 0.35	0.81 (57)
00031216011	2008-07-26 14:43:01	4674.11321	1969	PC*	1.47 ± 0.06	6.23 ± 0.36	1.31 (69)
00031216012	2008-07-29 00:32:00	4676.52222	1769	WT	1.65 ± 0.05	7.07 ± 0.30	0.99 (117)
00031216013	2008-07-30 11:52:00	4677.99444	1939	PC*	1.49 ± 0.07	6.88 ± 0.42	0.81 (61)
00031216014	2008-08-01 00:25:01	4679.51737	1963	PC*	1.54 ± 0.07	5.56 ± 0.34	0.98 (58)
00031216017	2008-08-01 11:37:30	4679.98438	1999	WT	1.61 ± 0.07	7.77 ± 0.44	1.50 (84)
00031216015	2008-08-03 10:34:01	4681.94029	2043	PC*	1.54 ± 0.08	5.83 ± 0.38	0.82 (55)
00031216016	2008-08-04 07:19:01	4682.80487	1915	PC*	1.53 ± 0.09	4.53 ± 0.34	1.23 (44)
00031216018	2008-08-05 21:41:01	4684.40348	380	PC*	1.64 ± 0.20	$5.59^{+0.91}_{-0.82}$	Cash
00031216019	2008-08-06 07:19:01	4684.80487	2276	PC*	1.60 ± 0.08	5.04 ± 0.33	1.02 (54)
00031216020	2008-08-07 20:44:01	4686.36390	1803	PC*	1.61 ± 0.09	5.20 ± 0.39	1.02 (38)
00031216021	2008-08-08 12:47:01	4687.03265	4217	PC*	1.64 ± 0.06	5.34 ± 0.26	1.17 (89)
00031216022	2008-08-10 01:47:01	4688.57432	2753	PC*	1.62 ± 0.09	5.56 ± 0.43	1.08 (35)
00031216023	2008-08-12 06:32:01	4690.77223	2190	PC*	1.55 ± 0.07	5.31 ± 0.32	1.18 (62)
00031216024	2008-08-14 04:52:00	4692.70278	1355	PC*	1.52 ± 0.13	4.10 ± 0.44	1.38 (21)
00031216025	2008-08-15 01:47:01	4693.57432	1649	PC*	1.63 ± 0.10	4.22 ± 0.34	0.98 (33)
00031216026	2008-08-16 21:07:01	4695.37987	1969	PC*	1.59 ± 0.08	5.19 ± 0.35	1.04 (50)
00031216027	2008-08-17 16:43:00	4696.19653	2425	PC*	1.61 ± 0.07	5.72 ± 0.32	0.80 (66)
00031216029	2008-08-20 08:59:01	4698.87432	1846	PC*	1.40 ± 0.07	4.72 ± 0.33	0.90 (51)
00031216030	2008-08-21 02:20:01	4699.59723	2095	PC*	1.61 ± 0.08	4.90 ± 0.34	1.08 (44)
00031216031	2008-08-22 10:28:01	4700.93612	1975	PC*	1.54 ± 0.08	4.64 ± 0.32	1.13 (46)
00031216032	2008-08-23 08:58:01	4701.87362	2155	PC*	1.57 ± 0.07	5.68 ± 0.34	1.41 (63)
00031216033	2008-08-24 14:20:01	4703.09723	538	PC*	$1.58^{+0.21}_{-0.20}$	$4.97^{+0.78}_{-0.76}$	1.30 (11)
00031216034	2008-08-25 09:37:01	4703.90071	335	PC*	1.52 ± 0.18	$6.20^{+0.97}_{-0.89}$	Cash
00031216035	2008-08-26 20:45:00	4705.36458	1059	PC*	1.55 ± 0.12	4.91 ± 0.50	0.81 (23)
00031216036	2008-08-27 17:39:00	4706.23542	1957	PC*	1.53 ± 0.08	4.78 ± 0.35	0.86 (43)
00031216038	2008-08-29 19:22:01	4708.30696	1885	PC*	1.46 ± 0.09	3.99 ± 0.33	1.12 (37)
00031216039	2008-08-31 14:36:01	4710.10834	1597	PC*	1.51 ± 0.09	4.39 ± 0.34	1.19 (37)
00031216040	2008-09-01 19:41:01	4711.32015	1730	PC*	1.54 ± 0.09	4.64 ± 0.37	0.78 (37)
00031216041	2008-09-02 18:05:01	4712.25348	2863	PC*	1.52 ± 0.07	4.05 ± 0.26	1.05 (59)
00031216042	2008-09-03 05:15:01	4712.71876	2052	PC*	1.65 ± 0.08	4.59 ± 0.31	0.79 (44)
00031216043	2008-09-04 16:54:46	4714.20470	346	PC*	1.59 ± 0.22	$4.02^{+0.76}_{-0.68}$	Cash
00031216044	2008-09-05 01:00:01	4714.54168	1711	PC*	1.62 ± 0.09	4.83 ± 0.36	1.50 (42)
00031216046	2008-09-07 15:27:40	4717.14421	470	PC*	1.54 ± 0.16	$4.96^{+0.72}_{-0.66}$	Cash
00031216047	2008-09-08 10:33:00	4717.93958	2501	PC*	1.54 ± 0.07	5.03 ± 0.32	0.63 (52)
00090023001	2008-09-09 01:20:01	4718.55557	1815	PC*	1.51 ± 0.09	4.73 ± 0.37	1.22 (38)
00031216048	2008-09-10 17:32:01	4720.23057	1046	PC*	1.53 ± 0.12	6.44 ± 0.66	0.98 (23)
00031216049	2008-09-11 12:58:00	4721.04028	2001	PC*	1.56 ± 0.08	5.32 ± 0.35	1.04 (53)
00031216050	2008-09-12 20:58:01	4722.37362	1973	PC*	1.66 ± 0.08	5.80 ± 0.39	0.76 (47)
00031216051	2008-09-13 20:55:02	4723.37155	411	PC*	1.38 ± 0.16	$5.13^{+0.77}_{-0.70}$	Cash
00031216052	2008-09-16 15:03:00	4726.12708	837	PC*	1.51 ± 0.13	4.93 ± 0.52	0.98 (21)
00031216053	2008-09-17 16:29:01	4727.18682	894	PC*	1.56 ± 0.12	4.98 ± 0.52	0.99 (22)
00031216054	2008-09-23 05:36:01	4732.73334	3103	PC*	1.58 ± 0.08	3.93 ± 0.24	0.89 (61)
00031216055	2008-09-24 09:14:01	4733.88473	1387	PC*	1.66 ± 0.12	4.74 ± 0.44	0.89 (26)
00031216056	2008-09-25 02:34:01	4734.60696	2786	PC*	1.60 ± 0.07	4.43 ± 0.27	1.13 (58)
00031216057	2008-09-26 04:16:01	4735.67779	2725	PC*	1.55 ± 0.07	4.11 ± 0.25	0.70 (57)
00031216058	2008-09-27 04:22:00	4736.68194	2725	PC*	1.62 ± 0.08	3.75 ± 0.25	1.11 (48)
00031216059	2008-09-28 04:27:01	4737.68543	1797	PC*	1.57 ± 0.08	5.23 ± 0.35	0.93 (46)
00031216060	2008-09-29 03:08:01	4738.63057	2759	PC*	1.59 ± 0.06	5.81 ± 0.32	1.09 (73)
00031216061	2008-09-30 03:06:01	4739.62918	2594	PC*	1.60 ± 0.06	5.92 ± 0.32	1.29 (71)
00031216062	2008-10-01 04:42:00	4740.69583	3108	PC*	1.66 ± 0.06	6.00 ± 0.29	1.04 (86)
00031216063	2008-10-02 04:47:01	4741.69932	3107	PC*	1.64 ± 0.06	5.12 ± 0.27	1.20 (75)
00035030028	2008-10-05 13:06:01	4745.04584	1221	PC*	1.62 ± 0.13	4.09 ± 0.40	0.61 (23)
00035030029	2008-10-10 20:26:01	4750.35140	807	PC*	1.78 ± 0.16	$3.32^{+0.42}_{-0.38}$	Cash
00035030030	2008-10-26 20:25:01	4766.35071	428	PC*	$1.69^{+0.24}_{-0.23}$	$2.72^{+0.54}_{-0.47}$	Cash
00090023002	2008-12-25 04:53:00	4825.70347	1493	PC	1.62 ± 0.15	$1.39^{+0.16}_{-0.17}$	0.93 (16)

Table 3. continued.

ObsID	START	JD −2 450 000	Exp [s]	Mode	Γ	$F_{1\ \mathrm{keV}}$ [μJy]	$\chi^2/\nu\,(\nu)$
00090023003	2008-12-26 05:15:01	4826.71876	1522	PC	1.54 ± 0.13	$1.49^{+0.17}_{-0.16}$	0.66 (19)
00090023004	2008-12-27 16:31:01	4828.18821	1682	PC	1.77 ± 0.20	$0.99^{+0.16}_{-0.14}$	Cash
00090023005	2008-12-29 00:27:01	4829.51876	1331	PC	1.68 ± 0.16	$1.85^{+0.25}_{-0.23}$	Cash
00090023006	2008-12-30 05:24:00	4830.72500	1276	PC	1.46 ± 0.18	$1.10^{+0.16}_{-0.17}$	1.24 (12)
00090023007	2008-12-31 16:42:01	4832.19584	707	PC	$1.58^{+0.21}_{-0.22}$	1.37 ± 0.23	Cash
00090023008	2009-01-01 12:01:00	4833.00069	1131	PC	1.57 ± 0.21	1.28 ± 0.21	1.72 (10)
00035030031	2009-01-21 17:05:01	4853.21182	1436	PC	$1.59^{+0.19}_{-0.18}$	$1.34^{+0.22}_{-0.19}$	Cash
00035030032	2009-01-22 17:17:10	4854.22025	857	PC	$1.73^{+0.25}_{-0.23}$	$1.24^{+0.22}_{-0.21}$	Cash
00035030033	2009-01-23 06:10:01	4854.75696	634	PC	$1.70^{+0.27}_{-0.25}$	$1.58^{+0.31}_{-0.28}$	Cash
00035030034	2009-01-24 15:46:01	4856.15696	485	PC	$1.80^{+0.25}_{-0.24}$	$1.66^{+0.31}_{-0.29}$	Cash
00035030035	2009-01-25 06:32:00	4856.77222	927	PC	1.70 ± 0.16	$1.44^{+0.20}_{-0.18}$	Cash
00035030036	2009-01-26 08:14:01	4857.84307	924	PC	1.78 ± 0.19	$1.75^{+0.24}_{-0.25}$	1.26 (11)
00035030037	2009-01-27 11:32:01	4858.98057	991	PC	1.67 ± 0.18	$1.43^{+0.22}_{-0.21}$	0.96 (10)
00035030038	2009-05-23 03:25:01	4974.64237	4137	PC*	1.56 ± 0.07	2.46 ± 0.16	1.05 (52)
00035030039	2009-05-24 22:38:01	4976.44307	3805	PC*	1.62 ± 0.07	3.62 ± 0.20	0.92 (70)
00035030040	2009-05-26 16:30:00	4978.18750	4061	PC*	1.58 ± 0.06	3.31 ± 0.19	1.17 (67)
00031018009	2009-08-12 07:42:01	5055.82084	837	PC*	1.65 ± 0.14	4.45 ± 0.50	1.20 (16)
00090081001	2009-08-13 12:55:01	5057.03821	2101	PC*	1.75 ± 0.08	5.09 ± 0.33	1.17 (46)
00035030041	2009-08-14 00:09:01	5057.50626	1033	PC*	1.74 ± 0.12	$4.58^{+0.47}_{-0.46}$	1.39 (20)
00035030042	2009-08-15 01:47:02	5058.57433	1961	PC*	1.70 ± 0.09	4.88 ± 0.34	0.73 (41)
00035030043	2009-08-16 11:17:01	5059.97015	451	PC*	$1.85^{+0.19}_{-0.18}$	$4.73^{+0.68}_{-0.63}$	Cash
00035030044	2009-08-17 09:55:00	5060.91319	1783	PC*	1.70 ± 0.10	4.36 ± 0.35	0.71 (32)
00035030045	2009-08-18 00:19:01	5061.51321	2178	PC*	1.54 ± 0.08	4.04 ± 0.29	1.06 (43)
00035030046	2009-08-19 08:27:01	5062.85209	1367	PC*	1.76 ± 0.12	4.59 ± 0.43	0.68 (24)
00035030047	2009-08-19 13:30:00	5063.06250	812	PC*	1.62 ± 0.14	3.96 ± 0.49	1.31 (15)
00035030048	2009-08-20 06:55:01	5063.78821	1923	PC*	1.66 ± 0.08	4.70 ± 0.34	0.75 (40)
00035030049	2009-08-21 21:33:00	5065.39792	1096	PC*	1.68 ± 0.13	4.33 ± 0.45	0.92 (21)
00035030050	2009-08-22 19:57:52	5066.33185	1826	PC*	1.51 ± 0.08	5.71 ± 0.38	1.20 (49)
00035030051	2009-08-23 08:47:00	5066.86597	2066	PC*	1.51 ± 0.07	6.70 ± 0.40	1.01 (63)
00035030052	2009-08-24 08:55:01	5067.87154	2021	PC*	1.51 ± 0.06	6.11 ± 0.36	1.20 (63)
00035030053	2009-08-25 08:48:00	5068.86667	1517	PC*	1.51 ± 0.09	7.02 ± 0.51	1.05 (47)
00035030054	2009-08-26 21:59:00	5070.41597	1559	PC*	1.47 ± 0.06	9.22 ± 0.53	0.68 (71)
00035030055	2009-08-27 09:01:01	5070.87571	1573	PC*	1.38 ± 0.07	8.25 ± 0.53	0.75 (64)
00035030056	2009-08-28 09:15:01	5071.88543	1637	PC*	1.39 ± 0.07	8.85 ± 0.54	1.08 (67)
00035030057	2009-08-29 09:10:01	5072.88196	1692	PC*	1.57 ± 0.06	9.06 ± 0.48	0.98 (75)
00035030058	2009-08-30 15:42:01	5074.15418	2601	PC*	1.45 ± 0.05	7.80 ± 0.36	1.06 (102)
00035030059	2009-08-31 15:47:01	5075.15765	2074	PC*	1.50 ± 0.06	8.56 ± 0.43	1.01 (91)
00035030060	2009-09-01 14:17:00	5076.09514	2003	PC*	1.52 ± 0.06	7.82 ± 0.40	1.13 (82)
00035030061	2009-09-02 17:55:42	5077.24701	2124	PC*	1.52 ± 0.06	8.66 ± 0.43	0.94 (91)
00035030062	2009-09-03 06:54:01	5077.78751	963	PC*	1.55 ± 0.09	8.86 ± 0.72	0.91 (37)
00035030063	2009-09-06 19:51:01	5081.32709	1647	PC*	1.63 ± 0.07	7.11 ± 0.44	0.86 (54)
00035030064	2009-09-07 18:23:01	5082.26598	1467	PC*	1.44 ± 0.09	5.71 ± 0.47	1.14 (38)
00035030065	2009-09-08 23:15:01	5083.46876	1442	PC*	1.45 ± 0.08	7.68 ± 0.55	0.93 (46)
00035030066	2009-09-09 00:56:01	5083.53890	2116	PC*	1.49 ± 0.08	5.44 ± 0.40	0.84 (44)
00090081002	2009-09-13 20:33:47	5088.35679	1993	PC*	1.55 ± 0.06	9.53 ± 0.53	1.22 (70)
00035030067	2009-09-16 22:15:01	5091.42709	1503	PC*	1.61 ± 0.06	9.89 ± 0.54	1.04 (71)
00031493001	2009-09-17 04:29:43	5091.68730	1999	WT	1.51 ± 0.04	11.38 ± 0.36	1.00 (211)
00031493003	2009-09-18 03:15:00	5092.63542	2509	PC*	1.58 ± 0.05	9.75 ± 0.40	1.16 (118)
00031493004	2009-09-19 13:06:00	5094.04583	2542	PC*	1.71 ± 0.05	8.02 ± 0.36	1.32 (94)
00031493005	2009-09-20 17:59:00	5095.24931	2389	WT2	1.65 ± 0.04	7.96 ± 0.28	1.08 (185)
00031493007	2009-09-22 00:26:01	5096.51807	1819	WT2	1.68 ± 0.05	9.11 ± 0.35	1.08 (157)
00031493008	2009-09-23 19:51:01	5098.32709	1578	WT	1.72 ± 0.05	8.36 ± 0.34	0.99 (116)
00031493009	2009-09-24 13:12:01	5099.05001	2109	WT3	1.66 ± 0.05	8.64 ± 0.34	1.19 (132)
00031493010	2009-09-25 06:52:00	5099.78611	2149	WT3	1.62 ± 0.05	7.66 ± 0.31	1.22 (137)
00031493011	2009-09-26 06:58:00	5100.79028	2144	WT3	1.64 ± 0.05	7.85 ± 0.33	1.00 (126)
00031493012	2009-10-06 03:08:00	5110.63056	3422	WT6	1.58 ± 0.03	11.28 ± 0.28	1.15 (285)
00031493013	2009-10-08 14:55:01	5113.12154	3416	WT5	1.63 ± 0.03	11.31 ± 0.27	1.12 (282)
00031493014	2009-10-09 21:28:00	5114.39444	2917	WT5	1.58 ± 0.03	12.33 ± 0.32	1.06 (265)
00090077001	2009-10-12 20:05:02	5117.33683	1958	WT4	1.64 ± 0.04	9.70 ± 0.36	0.95 (158)
00090077002	2009-10-13 00:32:01	5117.52223	1783	WT4	1.63 ± 0.04	9.41 ± 0.36	1.17 (148)
00090077003	2009-10-14 00:41:00	5118.52847	1838	WT5	1.66 ± 0.04	8.54 ± 0.39	1.01 (110)
00090077004	2009-10-15 00:43:01	5119.52987	1854	WT3	1.65 ± 0.04	8.38 ± 0.33	0.87 (130)
00090077005	2009-10-16 04:02:01	5120.66807	2114	WT3	1.65 ± 0.04	8.38 ± 0.33	0.87 (130)
00090077006	2009-10-17 00:55:01	5121.53821	1964	WT3	1.67 ± 0.04	9.70 ± 0.33	1.16 (185)
00090077007	2009-10-18 11:03:01	5122.96043	2119	WT2	1.64 ± 0.05	7.66 ± 0.30	1.22 (147)

Table 3. continued.

ObsID	START	JD $-2\,450\,000$	Exp [s]	Mode	Γ	$F_{1\ \mathrm{keV}}$ [μJy]	$\chi^2/\nu\,(\nu)$
00090077008	2009-10-19 02:44:00	5123.61389	539	WT2	1.70 ± 0.09	7.60 ± 0.58	1.20 (41)
00090077009	2009-10-20 06:21:01	5124.76459	1868	WT4	1.62 ± 0.05	7.51 ± 0.31	0.96 (134)
00090077010	2009-10-21 15:55:01	5126.16321	495	WT	1.68 ± 0.09	8.82 ± 0.63	1.16 (44)
00090077011	2009-10-22 19:25:01	5127.30904	2054	WT2	1.75 ± 0.04	11.27 ± 0.35	1.23 (191)
00090077012	2009-10-23 00:27:01	5127.51876	4922	WT6	1.68 ± 0.02	11.27 ± 0.23	1.18 (318)
00090077013	2009-10-24 00:01:01	5128.50071	1638	WT4	1.67 ± 0.05	8.41 ± 0.34	0.87 (125)
00090077014	2009-10-25 19:41:00	5130.32014	2124	WT2	1.67 ± 0.04	8.15 ± 0.30	1.01 (155)
00035030068	2009-10-31 12:08:01	5136.00557	1429	WT2	1.65 ± 0.06	7.25 ± 0.34	0.76 (99)
00035030069	2009-11-04 17:38:02	5140.23475	801	WT4	1.78 ± 0.09	7.48 ± 0.48	1.29 (57)
00035030070	2009-11-06 23:56:00	5142.49722	1015	WT	1.64 ± 0.08	6.23 ± 0.39	0.95 (66)
00035030071	2009-11-11 17:45:00	5147.23958	1080	WT	1.78 ± 0.08	6.20 ± 0.37	1.00 (66)
00035030072	2009-11-18 02:33:01	5153.60626	1144	WT	1.62 ± 0.07	6.48 ± 0.37	0.79 (75)
00035030073	2009-11-27 20:49:01	5163.36737	940	WT	1.52 ± 0.06	8.87 ± 0.48	1.03 (88)
00035030074	2009-12-01 16:35:01	5167.19098	1065	WT	1.56 ± 0.05	13.71 ± 0.54	1.11 (138)
00035030075	2009-12-02 00:28:01	5167.51946	1174	WT	1.53 ± 0.04	15.30 ± 0.53	1.20 (166)
00035030076	2009-12-03 15:22:01	5169.14029	985	WT	1.56 ± 0.05	15.42 ± 0.60	1.10 (139)
00035030077	2009-12-04 00:39:01	5169.52709	2759	WT2	1.49 ± 0.02	16.88 ± 0.37	1.09 (328)
00035030078	2009-12-05 13:37:38	5171.06780	645	WT	1.50 ± 0.05	13.83 ± 0.67	1.07 (92)
00035030079	2009-12-06 00:54:01	5171.53751	1079	WT2	1.62 ± 0.05	13.79 ± 0.59	1.00 (117)
00035030080	2009-12-07 23:23:01	5173.47432	1114	WT	1.51 ± 0.04	13.73 ± 0.52	1.36 (145)
00035030081	2009-12-08 21:53:01	5174.41182	1164	WT2	1.59 ± 0.04	13.58 ± 0.51	1.16 (143)
00035030082	2009-12-09 23:35:01	5175.48265	1100	WT	1.48 ± 0.04	12.43 ± 0.50	1.32 (130)
00035030083	2009-12-10 14:17:01	5176.09515	990	WT	1.60 ± 0.06	10.90 ± 0.51	0.92 (104)
00035030084	2009-12-11 09:20:01	5176.88890	1369	WT2	1.54 ± 0.05	9.68 ± 0.40	1.24 (126)
00035030085	2009-12-12 03:05:01	5177.62848	879	WT2	1.59 ± 0.08	8.07 ± 0.57	1.03 (57)
00035030086	2009-12-12 23:59:01	5178.49932	1325	WT2	1.57 ± 0.06	7.19 ± 0.37	0.87 (90)
00035030087	2009-12-14 01:35:01	5179.56598	1344	WT3	1.62 ± 0.05	8.00 ± 0.37	0.94 (106)
00035030088	2009-12-15 03:18:01	5180.63751	924	WT2	1.56 ± 0.07	7.81 ± 0.50	1.24 (68)
00035030089	2009-12-16 03:23:01	5181.64098	1194	WT2	1.56 ± 0.06	7.37 ± 0.40	1.14 (93)
00035030090	2009-12-18 00:22:01	5183.51529	1374	WT	1.59 ± 0.06	8.17 ± 0.39	0.86 (110)
00035030091	2009-12-19 11:45:01	5184.98959	1255	WT	1.73 ± 0.08	10.98 ± 0.73	0.86 (61)
00035030093	2009-12-21 02:15:01	5186.59376	1104	WT	1.52 ± 0.06	8.38 ± 0.42	1.49 (98)
00035030094	2009-12-22 10:22:00	5187.93194	1110	WT	1.61 ± 0.06	8.44 ± 0.42	1.09 (95)
00035030095	2009-12-25 07:46:01	5190.82362	1220	WT	1.62 ± 0.09	6.98 ± 0.56	1.08 (47)
00035030096	2009-12-26 01:06:00	5191.54583	1154	WT	1.48 ± 0.08	7.16 ± 0.51	1.08 (60)
00035030097	2009-12-26 23:59:01	5192.49932	869	WT	1.62 ± 0.08	8.12 ± 0.53	0.79 (64)
00035030098	2009-12-28 01:37:01	5193.56737	1200	WT	1.63 ± 0.06	7.73 ± 0.41	1.04 (88)
00035030099	2010-01-01 20:56:01	5198.37223	1109	WT2	1.67 ± 0.06	9.47 ± 0.45	1.02 (98)
00035030100	2010-01-08 01:02:01	5204.54307	1065	WT	1.60 ± 0.08	6.52 ± 0.43	0.94 (64)
00035030102	2010-01-17 19:11:01	5214.29932	2394	WT3	1.63 ± 0.03	10.68 ± 0.31	0.95 (221)